Vortex induced vibrations of a rotating circular cylinder at low Reynolds number

Ming Zhao, Liang Cheng, and Lin Lu

Articles you may be interested in

Numerical simulation of vortex-induced vibration of a circular cylinder in a spanwise shear flow
Phys. Fluids **27**, 063101 (2015); 10.1063/1.4921882

An experimental investigation of vortex-induced vibration of a rotating circular cylinder in the crossflow direction
Phys. Fluids **27**, 067101 (2015); 10.1063/1.4921683

Vortex-induced vibration of a circular cylinder of finite length
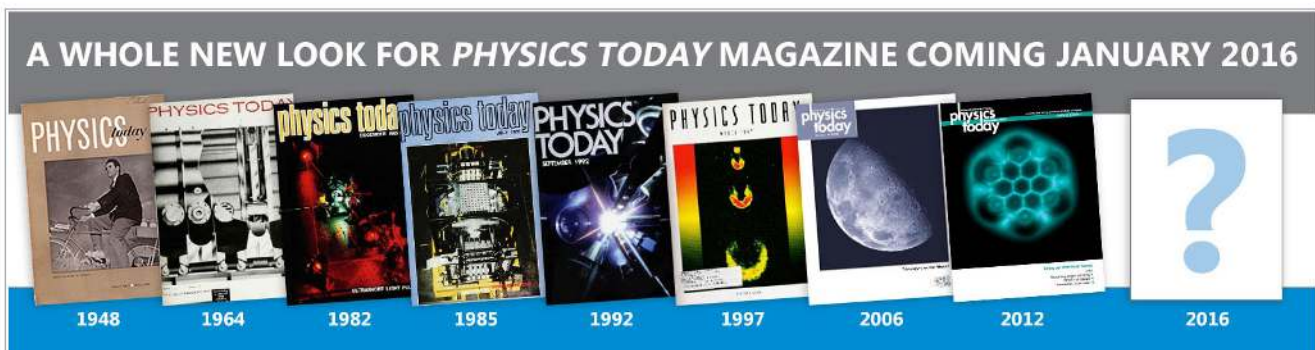Phys. Fluids **26**, 015111 (2014); 10.1063/1.4862548

Numerical simulation of vortex-induced vibration of two circular cylinders of different diameters at low Reynolds number
Phys. Fluids **25**, 083601 (2013); 10.1063/1.4816637

Numerical simulation of vortex-induced vibration of a square cylinder at a low Reynolds number
Phys. Fluids **25**, 023603 (2013); 10.1063/1.4792351

Vortex induced vibrations of a rotating circular cylinder at low Reynolds number

Ming Zhao,[1,a)] Liang Cheng,[2,3] and Lin Lu[4]

[1]*School of Computing, Engineering and Mathematics, University of Western Sydney, Locked Bag 1797, Penrith NSW 2751, Australia*
[2]*School of Civil, Environmental and Mining Engineering, The University of Western Australia, 35 Stirling Highway, Crawley WA 6009, Australia*
[3]*State Key Laboratory of Coastal and Offshore Engineering, Dalian University of Technology, Dalian 116024, China*
[4]*Center for Deepwater Engineering, Dalian University of Technology, Dalian 116024, China*

Vortex-induced vibration (VIV) of a rotating circular cylinder at a low Reynolds number of 150 and a low mass ratio of 2 is studied numerically. Simulations are conducted at three rotation rates of $\alpha = 0$, 0.5, and 1 and reduced velocities in the range of 1–13 with an interval of 0.2. The numerical results show that the rotation of the cylinder increases the response amplitude and widens the lock-in regime for the one-degree-of-freedom (1-dof) VIV in the cross-flow direction. The two-degree-of-freedom (2-dof) responses of the cylinder at $\alpha = 0.5$ and 1 are significantly different from that at $\alpha = 0$. For the 2-dof VIV, the response amplitude in the inline direction, which is much smaller than that in the cross-flow direction at $\alpha = 0$, is increased significantly at $\alpha = 0.5$ and 1. One initial branch is found at $\alpha = 0.5$ and two initial branches are found at $\alpha = 1$. In the initial branches, the response frequency locks onto a frequency that is smaller than the natural frequency of the cylinder and the response amplitude increases with the reduced velocity. The vortex shedding is found to be in the P+S mode for reduced velocities near the higher boundary of the initial branches and 2S mode in all other reduced velocity ranges for the 2-dof VIV. Simulations are conducted under both the increasing and decreasing reduced velocity conditions. A hysteresis region is found near the higher boundary of the lower branch for $\alpha = 0$, 0.5, and 1 in the 1-dof of VIV and for $\alpha = 0$ in the 2-dof VIV. The hysteresis region occurs near the higher boundary of the initial branches for $\alpha = 0.5$ and 1 in the 2-dof VIV. By analysing the component of the force coefficient that is in phase with the velocity of the cylinder, it is found that pressure force excites the vibration and the viscous force damps the vibration in both the inline and the cross-flow directions in the 2-dof VIV. The magnitude of the time averaged pressure and viscous force coefficients that are in phase with the velocities of the cylinder in the lock-in regime are found to be much greater than their counterparts outside the lock-in regime. © *2014 AIP Publishing LLC*. [http://dx.doi.org/10.1063/1.4886196]

I. INTRODUCTION

Vortex shedding flow in the wake of a circular cylinder in a fluid flow has been of interest in many studies due to its engineering importance. Flow in the wake of a circular cylinder transitions from two-dimensional (2D) to three-dimensional (3D) when the Reynolds number exceeds a critical value. The critical Reynolds numbers for the transition of the flow from 2D to 3D found in different studies differ slightly in the range of 140–190.[1] The Floquet stability analysis by Barkley and Henderson[2] showed that the 3D instability starts at a Reynolds number of about 188.5. Miller and Williamson[3]

---

a)Author to whom corresponding should be addressed. Electronic mail: m.zhao@uws.edu.au. Tel.: +61 2 4736 0085.

    26, 073602-1

found that the highest Reynolds number for laminar vortex shedding could be extended up to Re = 194 and even beyond 200 for a short period of time if the end effect is eliminated. The transition of the flow from 2D to 3D was intensively studied by many researchers.[2,4–9]

If a cylinder rotates in the fluid flow, the rotation speed of the cylinder affects the wake flow. In addition to the Reynolds number, flow past a rotating cylinder is also dependent on the rotation rate α, which is defined as the ratio of the rotating speed of the cylinder surface to the free stream velocity. Vortex shedding in the wake of a rotating cylinder was found to be fully suppressed if the rotation rate is greater than 2.[10–14] Early studies of flow past a rotating circular cylinder were focused on very low Reynolds numbers of Re $\leq$ 100.[15,16] Kang *et al.*[17] simulated flow past a rotating circular cylinder numerically at low Reynolds numbers and found that the critical rotation rates were about 1.4, 1.8, and 1.9 for Re = 60, 100, and 160, respectively, and the Strouhal number was nearly independent on the rotation rate. The large eddy simulation by Karabelas[18] showed that the vortex shedding for a high Reynolds number of 1.4×10^5 was suppressed at a rotation rate of 1.3.

Stojkovic *et al.*[19] found a second vortex shedding regime in the rotation speed range of 4.8 $\leq \alpha \leq$ 5.15 for Re = 100. The second vortex shedding mode is observed in the range of 4.85 $\leq \alpha \leq$ 5.17 for Re = 100 and is characterized by the shedding of one counterclockwise vortex from the upper part of the cylinder in one vortex shedding period.[20] Mittal and Kumar[21] and Lu *et al.*[22] found that, for Re = 200, the flow remained stable for 1.91 $\leq \alpha \leq$ 4.34 but lost its stability again for $\alpha \approx$ 4.35. The vortex shedding disappears again as the rotation ratio exceeds around 4.8. Lam[27] studied flow past a rotating cylinder at Re = 3600 to 5000 and $\alpha \leq$ 2.5 using flow visualization and PIV measurements. It was found that the wake became increasingly narrow and deflected sideways with the increasing cylinder rotation speed and the formation length of the vortices decreased with increasing α, leading to a slow increase in the vortex shedding frequency.

Three-dimensionality of flow past a rotating cylinder has also been studied. Mittal[28] found that the centrifugal instabilities existed along the entire span in a three-dimensional setup for a rotation rate of 5 and flow separation occurred near the cylinder ends due to the effect of the "no-slip" side-wall. The Direct Numerical Simulations (DNS) by Akoury *et al.*[29] showed that the rotation of the cylinder attenuated the three-dimensional instability and increases the critical Reynolds number for three-dimensionality. The flow was found to be three-dimensional at Re $\approx$ 220 for α = 0.5. Rao *et al.*[30] found that, while the three-dimensionality for $\alpha \leq$ 1 was similar to that of the non-rotating cylinder, the three-dimensional scenario at higher rotation rates became increasingly complex.

Vibration of a rotating circular cylinder in fluid flow has attracted less attention than that of a non-rotating circular cylinder. Extensive reviews of VIV of a circular cylinder can be found in Refs. 31–36. Large-amplitude oscillations of an elastically mounted cylinder in a fluid flow occur when the vortex shedding frequency synchronizes with the oscillation frequency of the cylinder.[37] The synchronization between the vortex shedding and the vibration of the cylinder is also called the "lock-in" or "lock-on" in literature. Lock-in occurs in a range of reduced velocities and the lock-in regime of the reduced velocity is dependent on the mass ratio and damping ratio of the system.[34,35] The mass ratio is defined as the ratio of the cylinder mass to the displaced fluid mass. The reduced velocity V_r is defined as $V_r = U/f_n D$, where U is the free-stream velocity, f_n is the structural natural frequency, and D is the cylinder diameter, which is measured in vacuum. The natural frequency of the free vibration of a cylinder in still water (defined as f_{nw} in this study) is used in many laboratory studies of VIV to define the reduced velocity, i.e., $V_r = U/f_{nw}D$.[38–41] In most of the numerical studies of VIV at low Reynolds numbers, the reduced velocity is defined using the structural natural frequency.[42,43] At high mass ratios, the structural natural frequency and the response frequency in fluid are essentially the same and the VIV frequency locks in with the natural frequency.[31,44] When the mass ratio is in the order of $O(1)$, the response frequency can be significantly greater than the natural frequency.[41]

Williamson and Roshko[37] found that the vortex-shedding pattern in the wake of a vibrating cylinder is related to the response mode of the cylinder. They conducted studies of a vibrating cylinder in fluid flow and used the number of the vortices that are shed from the cylinder to define the vortex shedding mode. For example, the 2P mode stands for two pairs of vortices being generated in one cycle of vibration and 2S mode stands for two single vortices being generated in one cycle

(a) Computational domain   (b) Finite element mesh near the cylinder
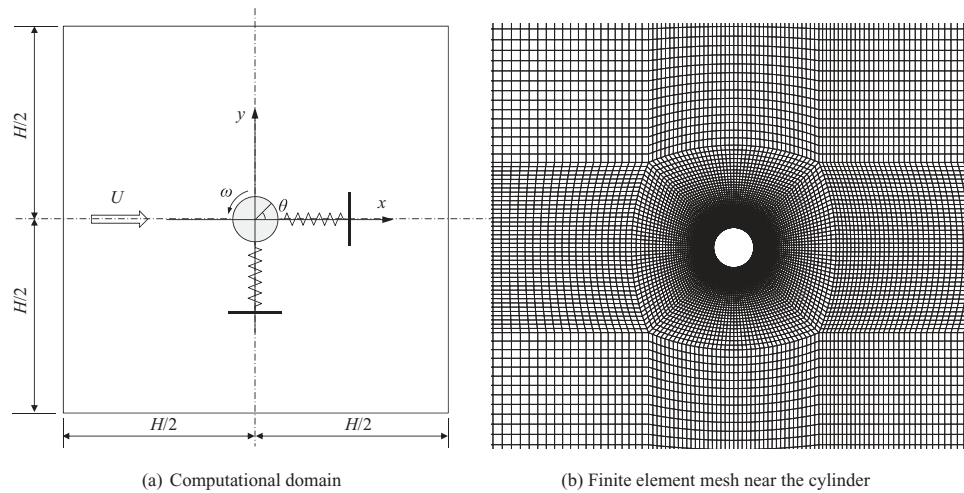
FIG. 1. Computational domain and computational mesh for flow past an elastically mounted rotating circular cylinder.

of vibration. For VIV of a circular cylinder in the cross-flow direction at low mass ratios, the vortex shedding is in the 2S mode in the initial branch and 2P mode in the upper and lower branch.[41] If the cylinder is allowed to vibrate both in the in-line and the cross-flow directions, the maximum response amplitude is increased to about 1.5 diameters of the cylinder and the velocity regime where the amplitude reaches its maximum is defined as super upper branch.[40] 2T mode (two triplets of vortices are shed from the cylinder in each vibration cycle) was observed when the amplitude is the maximum. For VIV of a circular cylinder at low Reynolds numbers in the laminar flow regime, the wake flow was found to be in the 2S mode throughout the lock-in regime.[42]

While flow past a rotating cylinder has been investigated extensively in the past, little attention has been paid to the influence of the rotation of the cylinder on the VIV. Rotating cylinder has been used for flow control around a non-vibrating cylinder.[22] Bourguet and Jacono[23] studied the one-degree-of-freedom (1-dof) flow-induced vibration of a rotating cylinder in the cross-flow direction for a low Reynolds number of 100 and investigated the impact of the symmetry breaking due to the imposed rotation on the VIV. In this study, the 1-dof and two-degree-of-freedom (2-dof) VIV of an elastically mounted rotating circular cylinder, as shown in Fig. 1(a), are investigated numerically by solving the two-dimensional Navier-Stokes equations using the finite element method. The rotation rate α is related to the angular velocity ω of the cylinder as $\alpha = \omega D/2U$. The vibration of the cylinder is calculated by solving the equation of the motion. Both the 1-dof VIV in the cross-flow direction only and the 2-dof VIV are studied. The study of VIV of a rotating cylinder is focused on a constant Reynolds number of 150, a constant mass ratio of 2, and low rotation rates of 0, 0.5, and 1.0. The numerical model is firstly validated against existing independent experimental and numerical results of flow past a rotating circular cylinder and 1-dof VIV of a rotating cylinder. Then the 1-dof and the 2-dof responses of the cylinder are discussed in detail separately.

II. NUMERICAL METHOD

The incompressible Navier-Stokes equations are solved by the Petrov-Galerkin finite element method (PG-FEM) to simulate the flow around a rotating cylinder. The finite element mesh is updated after each computational time step to accommodate the evolution of cylinder position. The Arbitrary Lagrangian Eulerian (ALE) method, which has been found to be an accurate method for simulating the VIV of cylinders in fluid flow,[45,46] is used in this study. The velocity (u, v), the time t, the length (x, y), and the pressure p are nondimensionalized as $(u, v) = (\tilde{u}, \tilde{v})/(f_n D)$, $t = \tilde{t} f_n$, $(x, y) = (\tilde{x}, \tilde{y})/D$, $p = \tilde{p}/(\rho f_n^2 D^2)$, respectively, where the tilde denotes the dimensional parameters and ρ is the fluid density. The non-dimensional ALE formulation of the NS equations

for incompressible flows is expressed as[45,46]

$$\frac{\partial u_i}{\partial t} + \left(u_j - u_{j,\text{mesh}}\right) \frac{\partial u_j}{\partial x_j} + \frac{\partial p}{\partial x_i} = \frac{V_r}{\text{Re}} \frac{\partial^2 u_i}{\partial x_j \partial x_j}, \tag{1}$$

$$\frac{\partial u_i}{\partial x_i} = 0, \tag{2}$$

where $x_1 = x$ and $x_2 = y$ are the Cartesian coordinates in the in-line and transverse directions of the flow, respectively; u_i is the fluid velocity component in the x_i-direction; t is the time; and $u_{i,\text{mesh}}$ is the velocity of the movement of the mesh nodes. The nondimensionalization method used in this study leads to a nondimensional free-stream velocity that is equal to the reduced velocity and a nondimensional vibration frequency that is equal to the ratio of the vibration frequency to the structural natural frequency. The nondimensional equation of the motion of the cylinder is

$$\ddot{X}_i + 4\pi\zeta\dot{X}_i + 4\pi^2 X_i = \frac{2}{\pi} \frac{V_r^2 C_{Fi}}{m^*}, \tag{3}$$

where $X_1 = X$ and $X_2 = Y$ are the displacements of the cylinder system in the inline and cross-flow directions, respectively; $\dot{X}_i$ and $\ddot{X}_i$ are the velocity and the acceleration of the cylinder, respectively; $m^* = m/m_d$ is the mass ratio with m being the mass of the cylinder and $m_d = \rho\pi D^2/4$ being the displaced mass of the fluid; $\zeta = c/\left(2\sqrt{km}\right)$ is the damping ratio with c and k being the damping constant and spring constant of the system, respectively; and $C_{F1} = C_D$ and $C_{F2} = C_L$ are the drag and lift coefficients, respectively, which are defined as $C_D = F_D/(\rho D U^2/2)$, $C_L = F_L/(\rho D U^2/2)$ with F_D and F_L being the drag and lift forces on the cylinder, respectively. The equations of motion, Eq. (3), are solved using the fourth-order Runge-Kutta algorithm.

After each computational time step in the numerical simulation, the position of the cylinder changes and each finite element node needs to be moved accordingly. The governing equation for calculating the displacements of the nodes of the FEM mesh is

$$\nabla \cdot (\gamma \nabla S_i) = 0, \tag{4}$$

where S_i represents the displacement of the nodal points in the x_i-direction and γ is a parameter that controls the mesh deformation. In order to avoid excessive deformation of the near-wall elements, the parameter γ in a finite element is set to be $\gamma = 1/A$, with A being the area of the element. By specifying the displacements at all boundaries, Eq. (4) is solved by the Galerkin FEM. The displacement S_i is the same as the displacement of the cylinder plus the rotation speed of the cylinder on the cylinder surface and zero on the rest of the boundaries.

A square rectangular computational domain of a boundary length of $200D$ is discretized into quadrilateral four-node linear finite elements. Figure 1(b) shows an example of the finite elements around the cylinders. Zhao et al.[47] simulated VIV of a cylinder at Re = 1000–15000 and found that if the width of the computational domain to the cylinder diameter ratio is greater than 10, the effects of the side boundaries on the results have been negligibly weak in the lock-in regime. Prasanth et al.[48] found that the blockage factor (the diameter to the domain width ratio) must be no more than 1% in order to obtain accurate results for Re $\leq$ 150. It is expected that the blockage factor of 0.5% used in this study will be small enough to eliminate the effects from the domain size on the numerical results. Initially, the velocity and the pressure in the whole computational domain are set to zero. The non-dimensional velocity at the inlet boundary is V_r and the velocity at the cylinder surfaces equals to the sum of translational and rotational velocities of the cylinder surface. At the outlet boundary, the pressure and the gradient of velocity in the inline direction are set to zero. At the two lateral boundaries, the gradient of the pressure and the velocity in the cross-flow direction are set to zero.

III. VALIDATION AND MESH DEPENDENCY STUDY

Simulations of flow past a rotating non-vibrating cylinder are conducted and the results of the velocity, pressure, and force coefficient are compared with the available data in published literature.
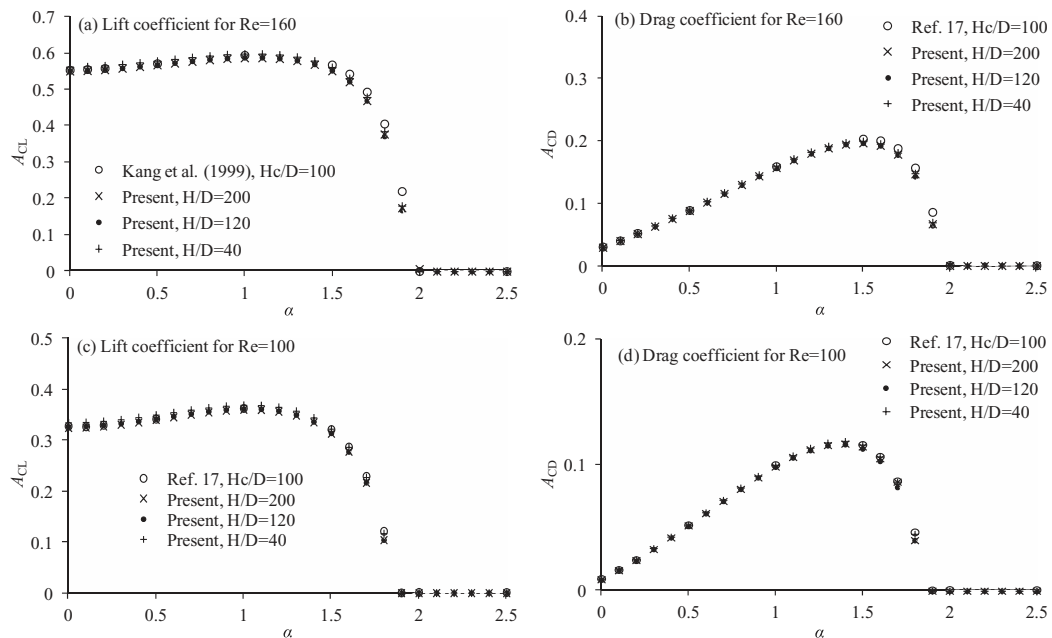
FIG. 2. Variations of amplitudes of the force coefficient of a non-vibrating rotating cylinder with the rotation rate.

For flow past a rotating circular cylinder, the computational domain size must be large enough to ensure that the results are convergent. Numerical results based on three meshes of different computational domain sizes of $H/D = 40$, 120, and 200 are compared with each other with H being the length of the side boundary of the domain as defined in Fig. 1(a). The computational domains for $H/D = 40$, 120, and 200 are divided into 15256, 35616, and 39196 four-node quadrilateral finite elements, respectively. There are 160 elements along the cylinder surface and the minimum mesh size in the radial direction is 0.002D. Figure 2 shows the comparison between the present results of the force coefficients for flow past a rotating cylinder at Re = 100 and 160 from the three meshes with the numerical results reported in Ref. 17, where a circular computational domain of a diameter of $H_c = 50D$ was used. A_{CD} and A_{CL} in Fig. 2 stand for the amplitudes of the drag and lift coefficients respectively. It can be seen that the results of the force coefficients at $H/D = 200$ are almost identical with those at $H/D = 120$, indicating the convergence of the results. The calculated force coefficients at $H/D = 40$ are slightly greater than those at $H/D = 200$ and 120 because of the stronger blockage effect. Present results agree well with those reported in Ref. 17. Judging by the zero amplitudes of the drag and lift coefficients, it can be confirmed that the vortex shedding is fully suppressed at α = 1.9 and 2.0 for Re = 100 and 160, respectively. The amplitude of the drag coefficient increases with α for $\alpha < 1.5$, while that of the lift coefficient changes little. The amplitudes of both the lift and drag coefficients decrease rapidly as α is increased from 1.5 to 2 for Re = 160 and from 1.5 to 1.9 for Re = 100. In this study, the mesh with $H/D = 200$ is used in all the subsequent simulations.

Simulation for Re = 200 and $\alpha = 0.5$ is conducted and the velocity distribution along the two radial lines of $\theta = 90°$ and $\theta = 0°$ (see Fig. 1(a) for the definition of θ) are compared with the experimental data reported in Ref. 49 and the numerical results published in Ref. 17 in Fig. 3. The cylinder and the fluid are initially stationary and given an impulsive fluid velocity and impulsive rotation speed. It can be seen that the flow velocity in the boundary layer changes quickly at the early stage of the flow. The present numerical results of the velocity distribution are almost identical with the numerical results in Ref. 17 and agree reasonably well with the experimental data. Flows past a cylinder at high rotation rates of $\alpha = 3$, 4, and 5, where the vortex shedding is suppressed, are also simulated and the results of the lift and drag coefficients are compared with other numerical results in Table I. Mittal and Kumar[21] used a square computational domain with a boundary length of $H = 100D$ and Padrino and Joseph[50] used a circular computational domain with a diameter of $H_c = 125D$. The agreement among the lift coefficient from the three studies is excellent. However,
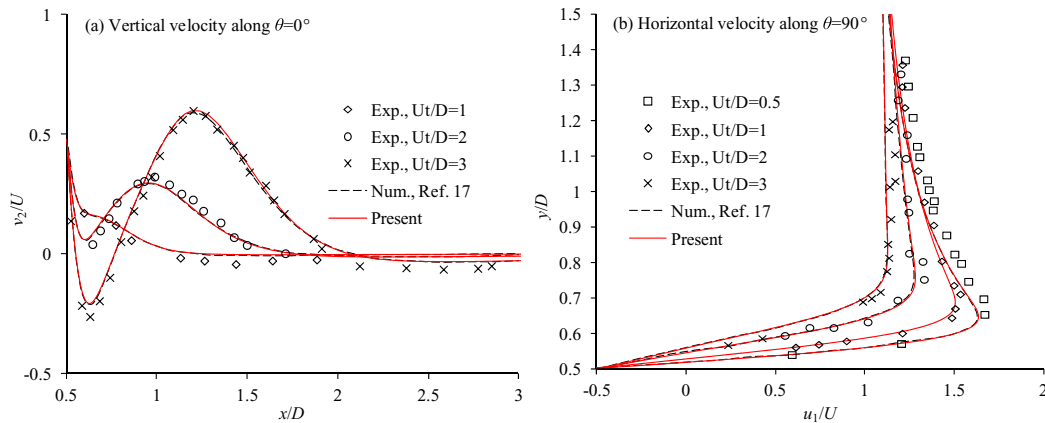
FIG. 3. Comparison of the numerical results of velocity profiles at Re = 200 and $\alpha = 0.5$ with the experimental data by Coutanceau and Menard.[49]

TABLE I. Comparison of the force coefficient from different models for Re = 200 and α = 3, 4, and 5.

α	3		4		5	
Force coefficient	C_L	C_D	C_L	C_D	C_L	C_D
Present (H/D = 200)	− 10.342	0.005	− 17.585	− 0.137	− 27.206	− 0.005
Mittal and Kumar (2003) (H/D = 100)	− 10.366	0.035	− 17.598	− 0.055	− 27.055	0.168
Padrino and Joseph (2006) (H_c/D = 125)	− 10.340	0.012	− 17.582	− 0.124	− 27.029	0.011

the drag coefficients obtained from different models are quite different. This is because the drag coefficients are extremely small and the relative errors are magnified.[50]

　　Figure 4 shows the comparison of the distribution of the pressure coefficient along the cylinder surface for Re = 200 and α = 3, 4, and 5. The pressure coefficient is defined as $C_P = (p - p_\infty)/(\rho U^2/2)$ with p_∞ being the pressure at the inlet boundary. The present results of pressure also agree well with those reported in Ref. 50. Because of the rotation of the cylinder, the pressure on the cylinder surface is very asymmetric, i.e., the difference between the pressures at $\theta = 90°$ and $270°$ increases with α. The increased pressure difference between the top and bottom sides of the cylinder at large α leads to an increase in the lift coefficient.

　　Table II shows the comparison among the Strouhal numbers from different numerical models for Re = 100 and α = 0, 0.5, 1, and 1.5. The Strouhal number is defined as $S_t = f_s D/U$ with f_s being
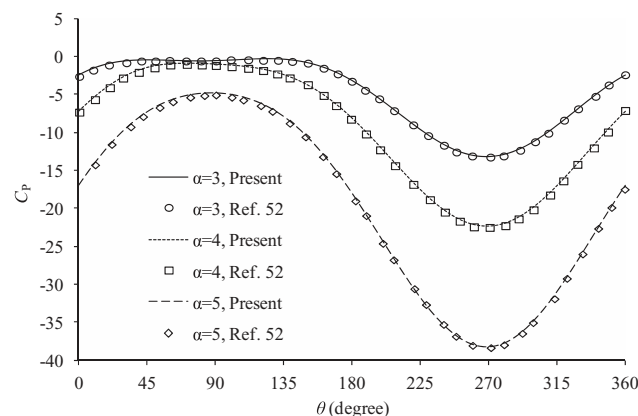

FIG. 4. Distribution of the pressure coefficient along the cylinder surface for Re = 200 and α = 3, 4, and 5.

TABLE II. Comparison of the Strouhal number for Re=100.

α	0	0.5	1	1.5
Present	0.1641	0.1645	0.1650	0.1630
Stojkovic et al.[51]	0.1650	0.1657	0.1658	0.1626
Pralits et al.[20]	0.1646	0.1647	0.1656	0.1634

the vortex shedding frequency, which is obtained based on the oscillation of the lift coefficient in this study. It can be seen that the rotation rate has a very small effect on the Strouhal number when it is less than 1.5. As the rotation rate is increased from 0 to 1.5, the Strouhal number is decreased from 0.1641 to 0.1630. The difference between present Strouhal number and any of the other three numerical results is less than 0.72% for α in the range of 0–1.5.

The present numerical model was previously used by the authors for the simulations of VIV of non-rotational cylinders. For validating the numerical model, Zhao and Yan[46] simulated VIV of a circular cylinder at a mass ratio of 10 and a Reynolds number of 100 and Zhao[45] simulated VIV of a circular cylinder at a mass ratio of $m^* = 2.546$ and Re = 150. The results of these two studies agree very well with those in Refs. 42, 52, and 53, respectively. To testify the validation of the numerical model on the VIV of a rotating cylinder, the 1-dof VIV of a rotating cylinder in the cross-flow direction for $m^* = 12.73$, Re = 100, and $\zeta = 0$ is simulated and the numerical results of the response amplitude and the mean (time-averaged) lift coefficients are compared with the numerical results by Bourguet and Jacono[23] in Fig. 5. Since the maximum rotation ratio studied in this paper is 1, the results for $\alpha = 0$, 0.5, 1, and 1.5 are compared with those in Ref. 23. Both the amplitudes and the mean lift coefficients agree with the numerical results in Ref. 23 very well. The lock-in range of the reduced velocity is found to increase with the rotation ratio. Similar to that of a stationary cylinder, the magnitude of the negative lift coefficient increases with the increase of the rotation rate of the cylinder.

When the lock-in occurs, the cylinder oscillates at a frequency that is related to the effective added mass, which is induced by the fluid force in phase with the acceleration of the cylinder.[25] Previous studies of the VIV of a cylinder have shown that the effective added mass coefficient may be very different from the potential flow value of 1.[23–26] The effective added mass coefficients in the x- and y-direction are defined as C_{mx} and C_{my}, respectively, and they can be calculated by[26]

$$C_{mx} = -\frac{2V_r^2}{\pi} \frac{\overline{C_i \ddot{X}}}{\overline{\ddot{X}^2}} \text{ and } C_{my} = -\frac{2V_r^2}{\pi} \frac{\overline{C_i \ddot{Y}}}{\overline{\ddot{Y}^2}}. \tag{5}$$

There is an extra term of V_r^2 in Eq. (5) compared with Eq. (5.13) in Ref. 23, because of the difference in the non-dimensionalization method for the time. The added mass coefficients for the rotation ratios of $\alpha = 1$ and 1.5 are compared with the calculated results by Bourguet and Jacono[23] in Fig. 6. The effective added mass coefficients calculated from the two numerical models are close
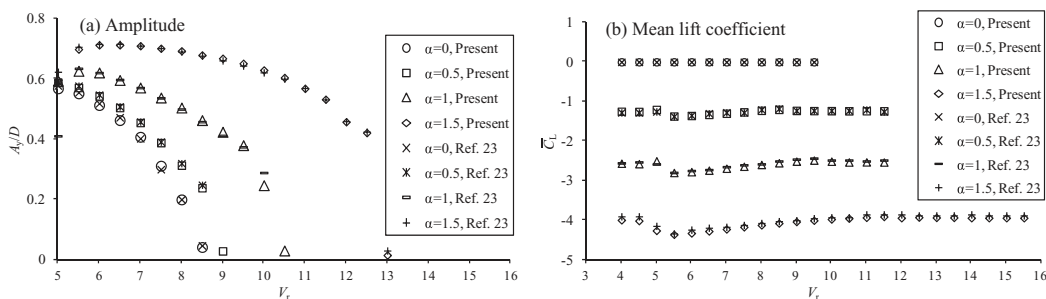

FIG. 5. Comparison between the present numerical of VIV of a cylinder for Re = 100, m* = 12.73, and $\zeta = 0$ with the numerical results in Ref. 23.
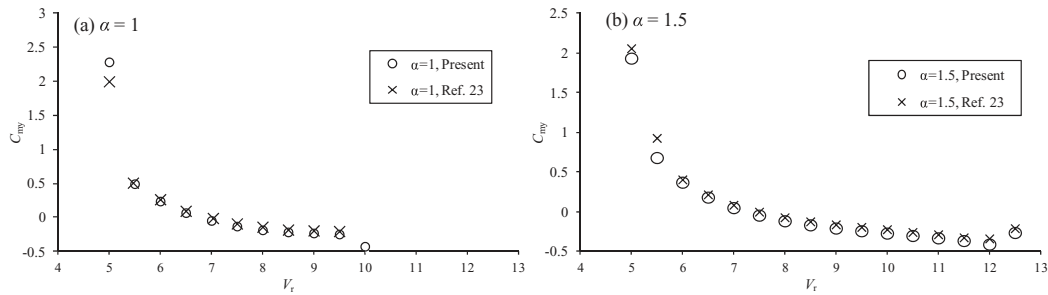
FIG. 6.   Comparison of the effective added mass coefficient.

to each other. As reported by Dahl *et al.*,[25] the effective added mass coefficient reduces with the increasing reduced velocity. It can be seen that the effective added mass coefficients are generally different from 1. The negative added mass coefficients are observed because of the out of phase between the lift coefficient and the displacement.

IV. ONE-DEGREE-OF-FREEDOM VIV OF A ROTATING CYLINDER

A. Response amplitude and frequency

One-degree-of-freedom VIV of a rotating cylinder is simulated at a constant Reynolds number of 150 and a constant mass ratio of $m^* = 2$. The cylinder is located at the centre of the square computational domain with a boundary length of $200D$. The structural damping ratio is set to zero in order to achieve large response amplitudes. Three rotation rates of $\alpha = 0$, 0.5, and 1 are considered and the reduced velocities range from 1 to 13 with an increment of 0.2. It has been found that the response of the cylinder at the reduced velocities near the low- and high-boundary of the lock-in regime exhibits hysteresis, i.e., the response of the cylinder depends on how the velocity is initialized. In the experimental study of 2-dof VIV of a circular cylinder in steady flow, Jauvtis and Williamson[40] investigated the VIV response of a cylinder under the increasing velocity (the velocity was gradually increased in the experiment) and decreasing velocity (the velocity was gradually decreased) conditions. It was found that the response amplitude of the cylinder under the increasing velocity condition is significantly greater than that under the decreasing velocity condition in the super upper branch. In many experimental studies, the reduced velocity was usually varied by keeping the structural natural frequency fixed and increasing the Reynolds number. In order to investigate the effect of the reduced velocity at a fixed Reynolds number, the structural natural frequency is varied in many numerical studies.[42, 48, 54] In this study, the Reynolds number is fixed at 150 and the simulations are conducted under both the increasing and decreasing reduced velocity conditions. In the increasing reduced velocity condition, the reduced velocity is 1 initially and after the equilibrium response is achieved, a new simulation is conducted by using the last computational step results as the initial conditions and increasing the reduced velocity by 0.2. Every time when the equilibrium response is achieved, the reduced velocity is increased by 0.2 again and the simulation is continued until the reduced velocity reaches to 13. In the decreasing reduced velocity condition, the reduced velocity is initially set to be 14 and is decreased by 0.2 after each equilibrium state is achieved until it is 1. After the reduced velocity is increased or decreased by 0.2, the simulations are conducted for enough long time to ensure at least 20 periods of equilibrium response are obtained.

Figure 7 shows the variation of the response amplitude in the cross-flow direction with the reduced velocity for $\alpha = 0$, 0.5, and 1. The response amplitude in the cross-flow direction is defined as $A_y = (Y_{\max} - Y_{\min})/2$, where the maximum and minimum displacements $Y_{\max}$ and $Y_{\min}$ in the cross-flow direction are obtained based on the time history of the cylinder displacement in 20 periods of vibration. The hysteresis response at the reduced velocities near the higher end of the lock-in regime can be clearly seen. However, the hysteresis is not obvious near the lower end of the lock-in regimes. In the numerical study by Singh and Mittal[42] for Re = 100 and $m^* = 10$, the hysteresis region of the reduced velocity near the lower end of the lock-in regime was very narrow (about 0.1).
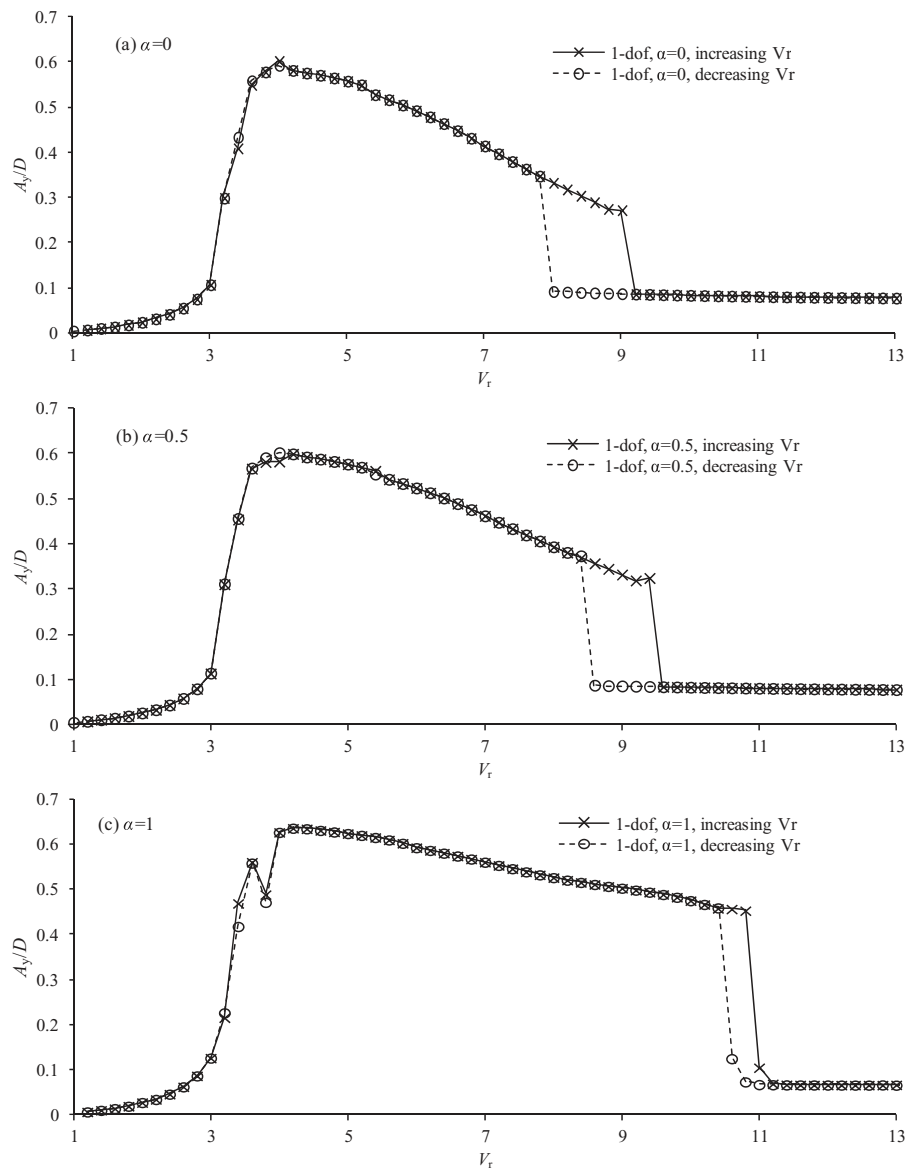
FIG. 7. Variation of the response amplitude with the reduced velocity for 1-dof VIV.

It is not observed in this study because the increment of the reduced velocity is 0.2, which is not small enough to capture the very narrow hysteresis region. Since this study is focused on the effects of the rotation rate on the response in a wide range of reduced velocity both in the 1-dof and 2-dof VIVs, efforts are not made to identify the very small region of hysteresis near the lower end of the lock-in regime. It is expected that the difference between the numerical results under the increasing and decreasing V_r conditions is only located in the very small reduced velocity range narrower than 0.20 near lower boundary lock-in regime. However, it can be seen in Fig. 7 that the hysteresis occurs at a wide range of reduced velocity near the higher end of the lock-in regime. The range of the reduced velocity for lock-in widens with the increase of the rotation ratio α. For $\alpha = 0$, 0.5, and 1, the higher boundaries of the lock-in regime under the increasing reduced velocity condition are 9, 9.4, and 10.8, respectively, and those under the decreasing reduced velocity condition are 7.8, 8.4, and 10.4, respectively. Outside the hysteresis region, the response amplitudes under the increasing V_r and decreasing V_r conditions are almost the same. When α is increased from 0 to 1, the maximum non-dimensional response amplitude is slightly increased from 0.60 to 0.64. However, the response
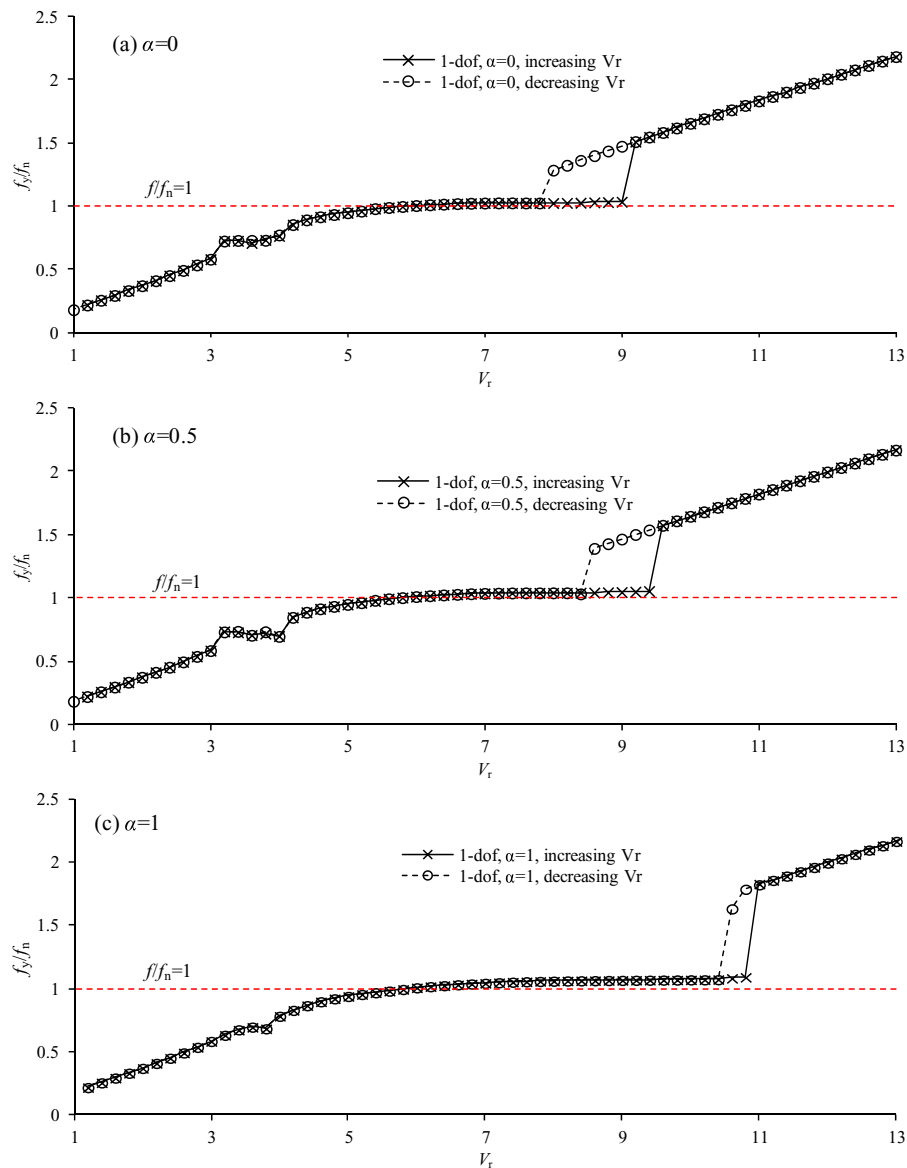
FIG. 8. Variation of the response frequency with the reduced velocity for 1-dof VIV.

amplitude near the higher boundary of the lock-in regime is increased significantly. For instance, the response velocity at $V_r = 9$ is increased from 0.27 to 0.50 after α is increased from 0 to 1. It can be seen in Fig. 7 that the difference in the response amplitude between $\alpha = 0.5$ and 1 is bigger than that between $\alpha = 0$ and 0.5, indicating that the change of the response amplitude with α become faster as α increases.

Figure 8 shows the comparison between the response frequencies under the increasing and decreasing V_r conditions for $\alpha = 0$, 0.5, and 1. Similar to the response amplitude, the response frequency under the increasing V_r condition is the same as that under the decreasing V_r condition, except in the hysteresis regions. The whole range of the reduced velocity can be divided into four regimes based on Fig. 8. In the regimes of $V_r \leq 3$ for $\alpha = 0$ and 0.5 and $V_r \leq 3.4$ for $\alpha = 1$, the response frequency increases with the reduced velocity linearly for all the three rotation ratios. In the regimes of $3.2 \leq V_r \leq 3.8$, $3.2 \leq V_r \leq 4$, and $3.6 \leq V_r \leq 3.8$ for $\alpha = 0$, 0.5, and 1, respectively, the response frequency locks onto a constant frequency which is lower than the natural frequency. In the third regime of the reduced velocity for each α, the non-dimensional response frequency f/f_n
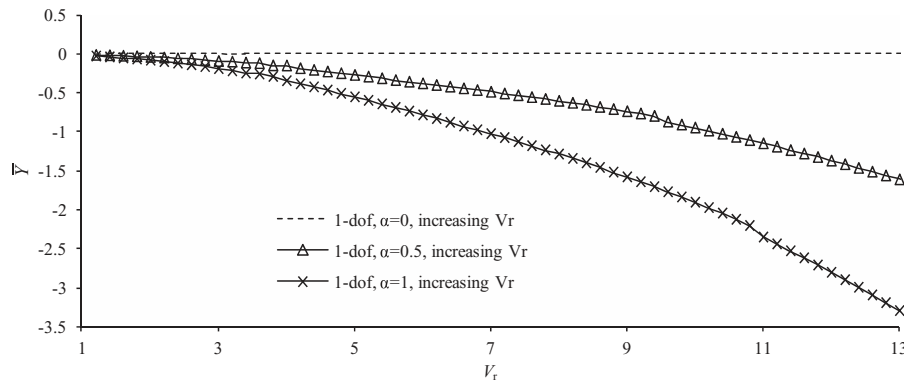
FIG. 9. Variation of the mean position of the cross-flow displacement with the reduced velocity under the increasing V_r condition for 1-dof VIV.

is close to 1. The Strouhal numbers for a non-vibrating rotating cylinder at $\alpha = 0$, 0.5, and 1 are very close to each other and they are $S_t = 0.1843$, 0.1840, and 0.1835, respectively. The reduced velocity corresponding to a natural frequency which is the same as the vortex shedding frequency is about 5.426, 5.435, and 5.450, respectively, for $\alpha = 0$, 0.5, and 1. It can be seen that when the reduced velocity is smaller than about 5.4, the response frequency of the cylinder does not exactly match the structural frequency, and the detuning increases as the reduced velocity moves away from about 5.4 (natural frequency moves away from the vortex shedding frequency of a non-vibrating cylinder). This phenomenon was referred to as soft-lock-in in Ref. 55. When the reduced velocity is greater than the higher boundary of the lock-in regime, the response amplitude becomes very small and the response frequency increases linearly with the increasing reduced velocity. A sudden jump in the response frequency occurs when the reduced velocity exceeds the higher boundary of the lock-in regime.

If the cylinder rotates, the mean position of the cylinder in the cross-flow direction moves in the negative y-direction and its magnitude increases with the increase of the reduced velocity. Figure 9 shows the variation of the mean position of the displacement in the cross-flow direction with the reduced velocity. The magnitude of the mean position of the cylinder increases with the increasing rotation rate. This is due to the increase in the magnitude of the mean lift coefficient, which has been found in Refs. 17 and 56 for a non-vibrating cylinder.

B. Force coefficients

It has been well known that the phase between the force and the vibration displacement in the cross-flow direction jumps from $0°$ to $180°$ at the boundary between the upper and lower branches.[39,40] For VIV of a cylinder, the fluid forces were found to only peak at the vibration frequency or at frequencies corresponding to higher harmonic of vibration frequency.[23] The higher harmonics in the forces also exist in the case of VIV of a non-rotating cylinder.[25,40] Bourguet and Jacono[23] decomposed both the displacement and the force into harmonics of the fundamental frequency of the displacement and examined the phase between the first harmonic components of the displacement and the force. In this study, the phase between the displacement and the force (defined as ψ_y) is examined by the correlation between the displacement and the force. The correlation between the displacement and the force in the x- and the y-directions is defined as

$$R_x = \overline{(X - \bar{X})(C_D - \bar{C}_D)}/(X'C_D') \text{ and } R_y = \overline{(Y - \bar{Y})(C_L - \bar{C}_L)}/(Y'C_L'), \qquad (6)$$

respectively, where the primes stand for the root mean square values and the over-bars stand for the averaging over time. The correlation coefficient is 1 if the displacement is in phase with the force and -1 if the displacement is out of phase with the force. Figure 10 shows the variation of the correlation coefficient between the Y-displacement and the lift coefficient for the 1-dof VIV in the increasing V_r condition. For all the three rotation ratios, the correlation coefficient is found to
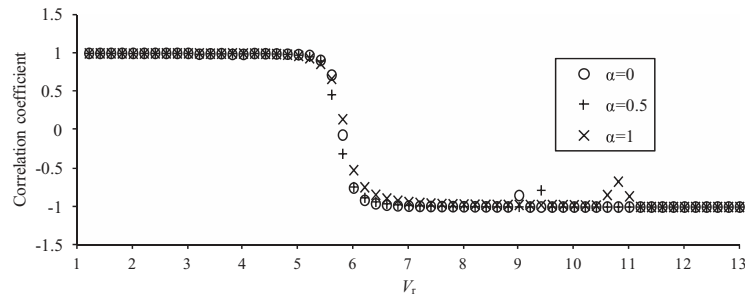
FIG. 10. Correlation between the displacement in the cross-flow direction and the lift coefficient for the 1-dof VIV in the increasing V_r condition.

change from 1 to -1 when the reduced velocity is increased from 5 to 6. If the structural damping is zero, the vibration frequency is lower than the natural frequency when $R_y \approx 1$ ($\psi_y = 0°$) and higher than the natural frequency when $R_y \approx -1$ ($\psi_y = 180°$).[35] It can be seen by comparing Fig. 8 with Fig. 10 that the vibration frequency exceeds the natural frequency when the correlation changes from 1 to -1.

For a damped system, part of the energy of the flow has to be transferred to the system to overcome the energy loss due the structural damping. Because the structural damping ratio is zero in this study, the net time averaged energy transferred from the flow to the system should be zero. However, the instantaneous energy transfer between the flow and the structure is found to oscillate with time.[23] A force excites the vibrations if it is in phase with the velocity of the cylinder, and damps the vibrations if it is out of phase with the velocity of the cylinder. Bourguet and Jacono[23] found that the force due to pressure (referred as pressure force) excites the vibration and the force due to viscosity (referred as viscous force) damps the vibration of the cylinder. In this study the contributions of the forces due to pressure and viscosity are quantified. The components of the total, the pressure, and the viscous lift coefficients that are in phase with the velocity of the cylinder are defined as C_{Lv}, C_{Lv}^p, and C_{Lv}^v, respectively, and they are calculated by

$$C_{Lv} = \frac{\sqrt{2}(C_L - \bar{C}_L)\dot{Y}}{\sqrt{\dot{Y}^2}}, C_{Lv}^p = \frac{\sqrt{2}(C_L^p - \bar{C}_L^p)\dot{Y}}{\sqrt{\dot{Y}^2}}, C_{Lv}^v = \frac{\sqrt{2}(C_L^v - \bar{C}_L^v)\dot{Y}}{\sqrt{\dot{Y}^2}}, \qquad (7)$$

where pressure and viscous lift coefficients (C_L^p and C_L^v) are obtained by integrating the pressure and the shear stress over the cylinder surface, respectively.

Figure 11 shows the variations of the time averaged coefficients $\bar{C}_L^p$ and $-\bar{C}_L^v$ with the reduced velocity for the 1-dof VIV in the increasing V_r condition. It is found that the pressure force always excites the vibration, while the viscous force always damps the vibration both inside and outside the lock-in regime. Because $\bar{C}_L^v$ is found to be always negative, $-\bar{C}_L^v$ is shown in Fig. 11 in order to compare the two force coefficients straightforwardly. It can be seen that both $\bar{C}_L^p$ and $-\bar{C}_L^v$ reach their maximum value at a same reduced velocity as the vibration amplitude of the cylinder does. $\bar{C}_L^p$ and $-\bar{C}_L^v$ outside the lock-in regime are very small, especially for reduced velocities higher than the upper boundary of the lock-in regime. $\bar{C}_L^p$ and $-\bar{C}_L^v$ are almost the same as each other in all the cases, leading to a zero net energy transfer from the fluid flow to the structure.

C. Vortex shedding flow

Figure 12 shows the vorticity contours of the wake flow under the increasing velocity condition for $\alpha = 0$ and 1 at the instants when the cylinder is at its highest position. The non-dimensional vorticity is defined as $\omega = (\partial v/\partial x - \partial u/\partial y)/V_r$. The vortex shedding for all the reduced velocities and rotation ratios is in the 2S mode, i.e., two single vortices are shed from the cylinder in one period of vibration. However, the vortex shedding patterns in different reduced velocities may be different from each other significantly. The reduced velocities in Figs. 12(a) and 12(d) are those when the response amplitudes reach its maximum. A negative vortex and a positive vortex are shed
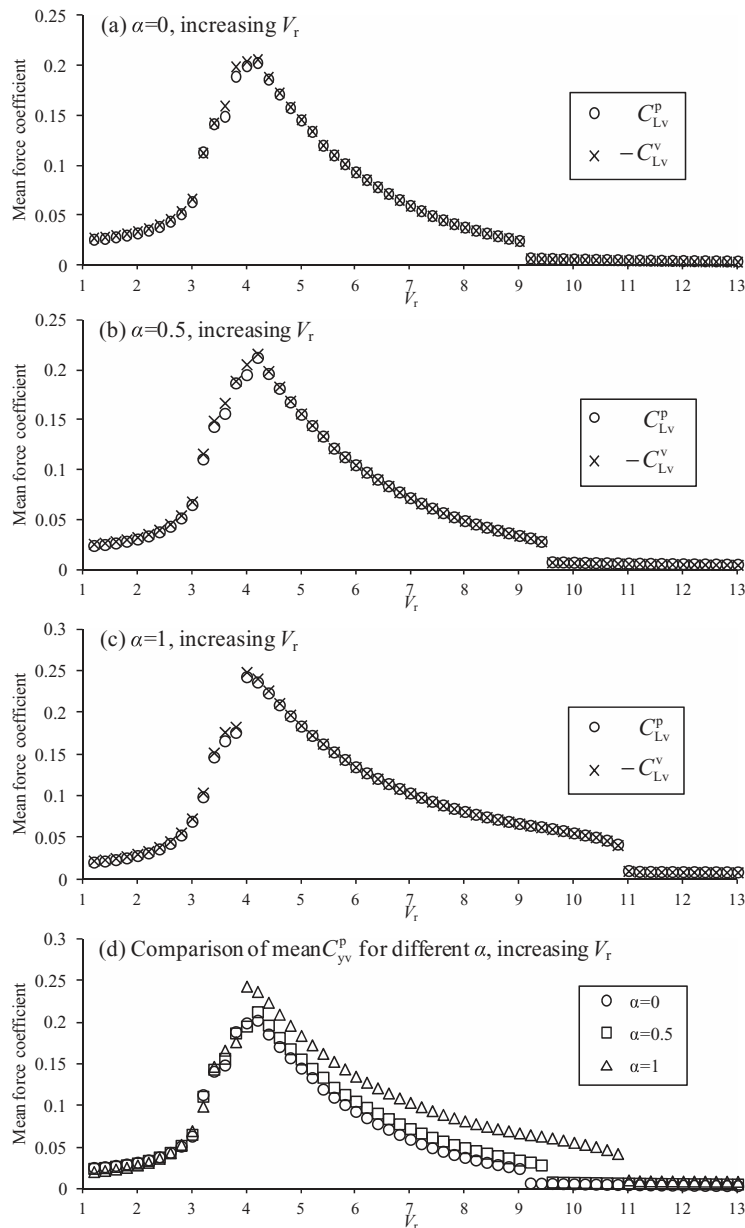
FIG. 11. The lift coefficients that are in phase with the velocity of the cylinder for the 1-dof VIV in the increasing V_r condition.

from the cylinder when the cylinder is at its highest and lowest positions, respectively. For $V_r = 4$, the vortex shedding patterns at $\alpha = 0$ and 1 are very similar to each other. In Figs. 12(a) or 12(d) the most upstream negative vortex in the top row is attached by a very weak positive vortex. This small positive vortex is very weak and dissipates very quickly. The vortex shedding patterns in Figs. 12(a) and 12(b) were similar to the $2P_O$ mode identified by Morese and Williamson.[57] The lift force is in phase with the displacement in the $2P_O$ mode and transfer positive energy to the cylinder, resulting in the maximum amplitude in the lock-in regime.

Figures 12(b) and 12(e) correspond to reduced velocities slightly smaller than the upper boundary of the lock-in regime. Compared with that in Figs. 12(a) and 12(c), the shear layers in Figs. 12(b) and 12(e) from the two sides extend further downstream before they form vortices. The vortices become elongated if the time taken by the shear layers to form vortices increases. The delay in
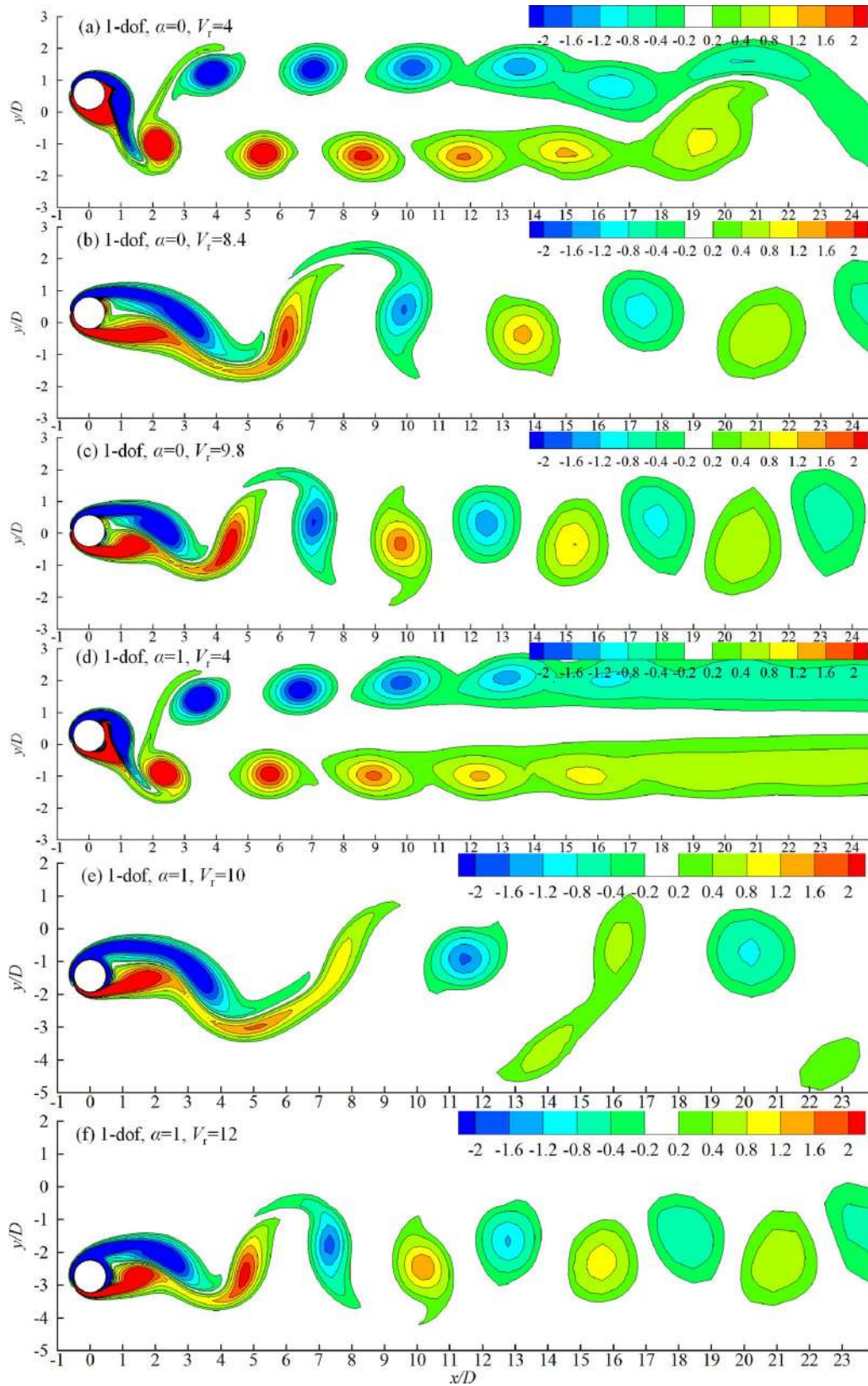
FIG. 12. Contours of the vorticity for the 1-dof VIV under the increasing velocity condition for $\alpha = 1$ and $V_r = 4$.

the formation of the vortices enables the vortex shedding frequency being locked onto the vibration frequency of the cylinder in a large range of the reduced velocity in the lock-in regime. The widening of the lock-in regime for a rotating cylinder is explained by examining the vortex shedding pattern shown in Fig. 12. When the cylinder rotates anticlockwisely, the relative velocity of the fluid at the bottom surface of the cylinder is reduced. The weakened shear layer postpones the timing of the formation of the positive vortices from the bottom surface of the cylinder. The elongation of the vortices shed from the bottom surface of the cylinder is a good indication of the delay in the formation of the vortices from the bottom surface of the cylinder. It is observed that each vortex from the bottom surface of the cylinder is so elongated that it is split into two while travelling downstream. Kang et al.[17] reported that the vortex shedding frequency reduced with the increasing rotation ratio at Re = 160 for a non-vibrating rotating cylinder. A slight change in the phase of vortex-induced force can lead to a change in the energy input from the vortices to the cylinder (sometimes from negative to positive).[57]

The reduced velocities in Figs. 12(c) and 12(f) are slightly higher than the upper boundary of the lock-in regime. The vortices in Figs. 12(c) and 12(f) are shed from the cylinder faster than those in Figs. 12(b) and 12(e) because more vortices are aligned downstream the cylinder. The vortex shedding patterns for $\alpha = 0.5$ are similar to those for $\alpha = 1$ and are not presented in Fig. 12. The difference between the vortices from the bottom surface and those from the top surface for $\alpha = 0.5$ is weaker than that for $\alpha = 1$ (Fig. 12(e)).

V. TWO-DEGREE-OF-FREEDOM VIV OF A ROTATING CYLINDER

A. Vibration amplitude and frequency

The input parameters for simulating the 2-dof VIV of a rotating cylinder are the same as those used in the 1-dof VIV, except that the cylinder is allowed to vibrate in both the inline and the cross-flow directions. The structural natural frequencies in the inline and cross-flow directions are the same. The *XY*-trajectories of the 2-dof vibration of the cylinder for $\alpha = 0$, 0.5, and 1 are shown in Fig. 13. For $\alpha = 0$, the vibration trajectories in the lock-in regime are in the shape of "8", except that at $V_r = 9$, the higher boundary of the lock-in regime. Based on the shape of the vibration trajectories, it is observed that the vibration frequency in the inline direction is twice that in the cross-flow direction for $\alpha = 0$. When the reduced velocity is outside the lock-in regime (for example, $V_r = 3$ and 10 in Fig. 13(a)), the cylinder almost vibrates only in the cross-flow direction with negligibly small amplitude in the inline direction. The trajectories of the cylinder in the lock-in regime for $\alpha = 0.5$ and 1 are similar to each other and are significantly different from those for $\alpha = 0$. If the cylinder rotates at $\alpha = 0.5$ and 1, the trajectory of the cylinder in one period of vibration comprises one single loop as shown in Figs. 13(b)–13(d). The single-loop trajectories suggest that the vibration frequency in the inline direction is the same as that in the cross-flow direction. It appears that the dimension of the *XY*-trajectory in the inline direction increases with α, indicating the increase of the inline amplitude. Some of the vibrations are not exactly periodic such as those at $V_r = 5$ for $\alpha = 0.5$ and at $V_r = 4$ and 5 for $\alpha = 1$. These reduced velocities are near the boundaries between two branches.

Figure 14 shows the variations of the response amplitudes in the inline and the cross-flow directions with the reduced velocity. The response amplitude in the inline direction is defined as $A_x = (X_{max} - X_{min})/2$ with X_{max} and X_{min} being the maximum and minimum displacements in the inline direction, respectively. Figure 15 shows the variation of the response frequency in the cross-flow direction with the reduced velocity for the 2-dof VIV. Similar to that of the 1-dof VIV, the hysteresis near the lower boundary of the lock-in regime is not obvious. Weak difference between the response amplitudes under the increasing and the decreasing V_r conditions is observed in the reduced velocity range between 3 and 4. For $\alpha = 0$, the response amplitude in the in-line direction is negligibly smaller than that in the cross-flow direction. This agrees with experimental observations at high Reynolds numbers in Refs. 40 and 58 and the numerical simulations at low Reynolds numbers in Refs. 42 and 59. The response amplitude reaches its maximum in the upper branch in the 2-dof VIV of a non-rotating cylinder.[35,38,39] The upper branch cannot be clearly identified
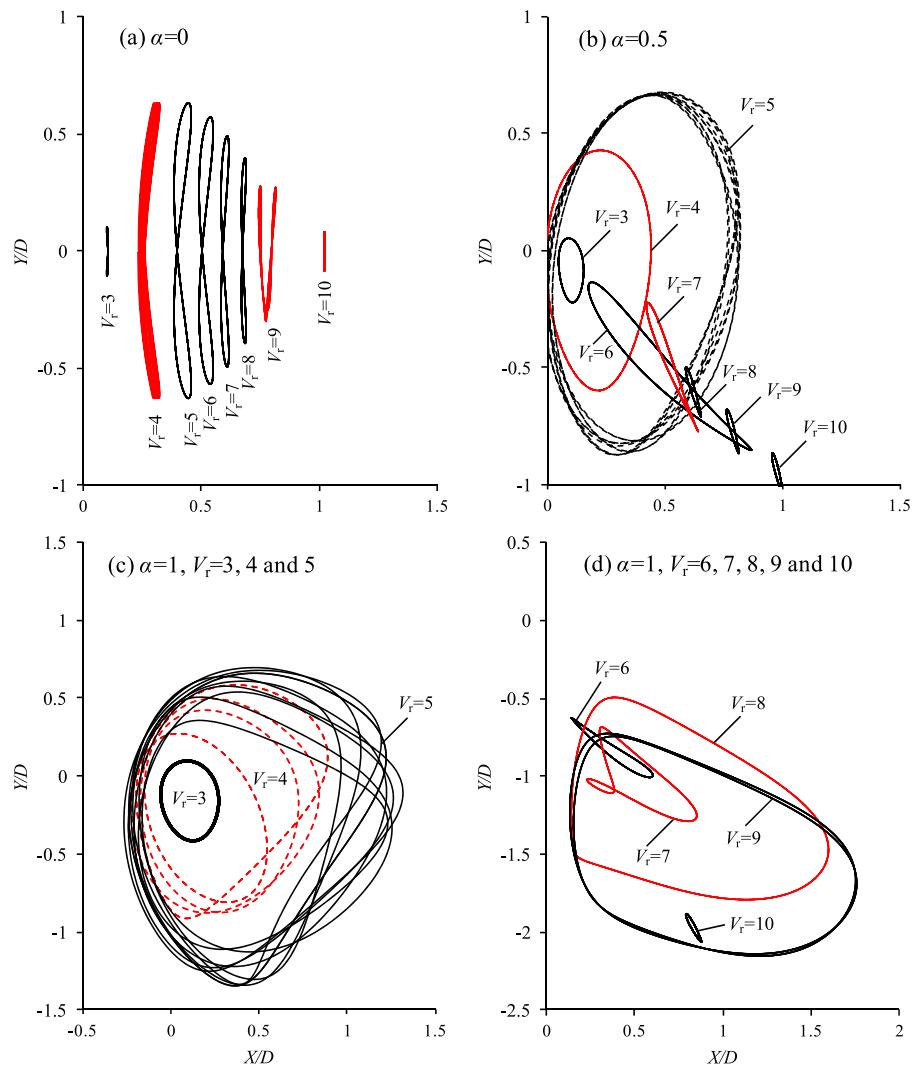
FIG. 13. XY-trajectory of the cylinder under the increasing V_r condition for the 2-dof VIV.

at low Reynolds numbers. Due to the wake vibration in the inline direction, the variation of the response amplitude with the reduced velocity in the cross-flow direction at $\alpha = 0$ for the 2-dof VIV is very similar to that for the 1-dof VIV. When the cylinder rotates at $\alpha = 0.5$ and 1, both the response amplitude and the response frequency are very different from those for a non-rotating cylinder ($\alpha = 0$). For $\alpha = 0.5$, the maximum response amplitude in the lock-in regime is increased significantly compared with that for $\alpha = 0$. It is about 0.65 at $\alpha = 0$ and is increased to 0.79 at $\alpha = 0.5$. For $\alpha = 1$, the maximum response amplitude is increased to 1.09. Anagnostopoulos and Bearman[60] conducted an experimental study of VIV of a cylinder at very low Reynolds numbers between 90 and 150 and reported that the maximum response amplitude occurred near the lower boundary of the lock-in regime, which is similar to what was observed in this study for $\alpha = 0$. However, when the rotation rate α is increased to 0.5, the maximum amplitude occurs in the middle of the lock-in regime. It is interesting to see that the response for $\alpha = 1$ includes two maximum response amplitudes. For both $\alpha = 0.5$ and 1, the disconnection in the variation of the response amplitude with the reduced velocity occurs after the response amplitude reaches its maximum value. Another striking difference between the responses of a rotating cylinder from that of a non-rotating cylinder is that the response amplitude in the inline direction is significantly increased in the lock-in regime.
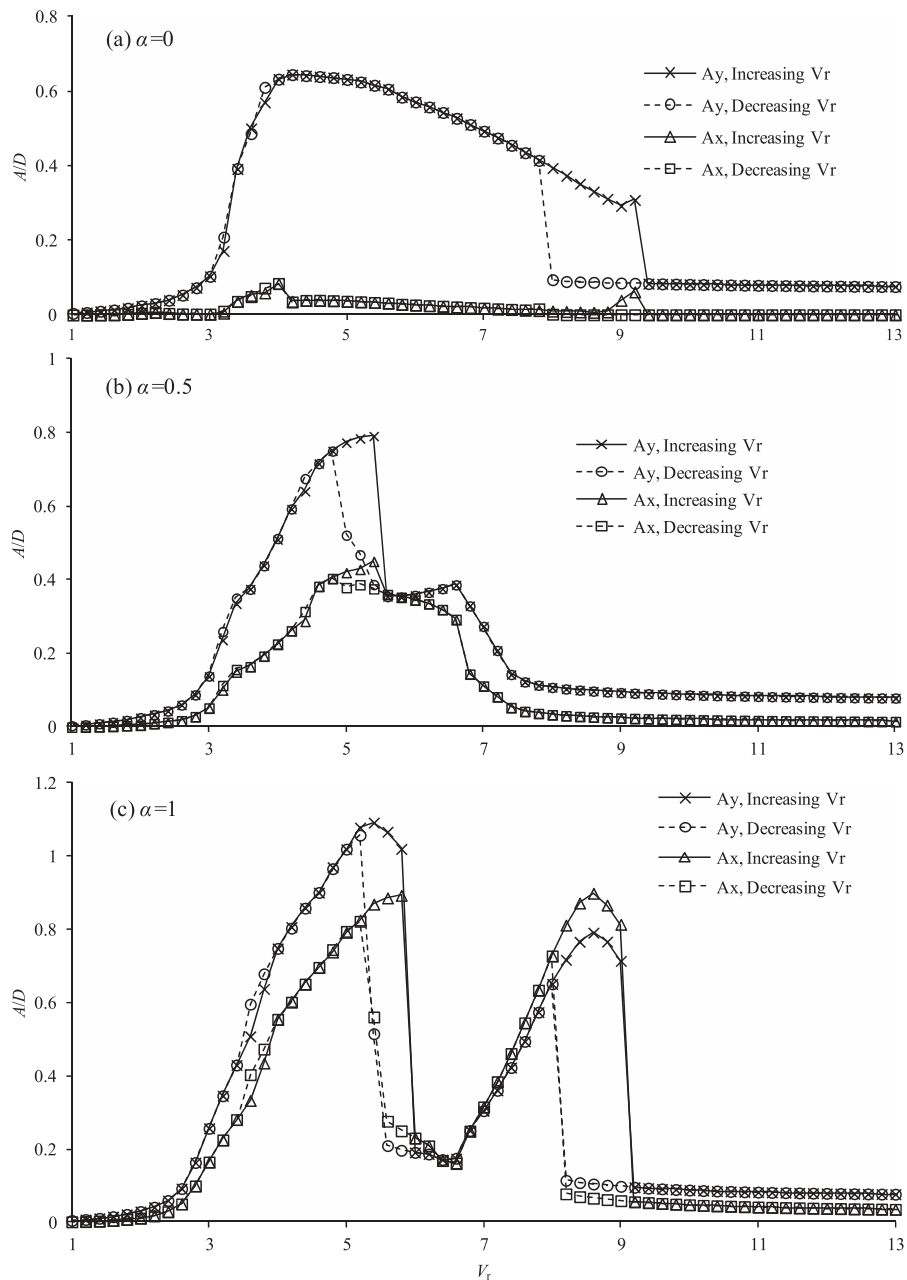
FIG. 14. Variation of the response amplitude with the reduced velocity for 2-dof VIV.

It can be seen from Fig. 15 that the response frequency locks onto a constant frequency which is smaller than the natural frequency in the range of $3.4 \leq V_r \leq 3.8$ and $3.2 \leq V_r \leq 5.4$ for $\alpha = 0$ and 0.5, respectively, for the increasing V_r condition. For $\alpha = 1$, the response frequency in the increasing V_r condition locks onto a constant frequency in two ranges: $3 \leq V_r \leq 5.8$ and $7 \leq V_r \leq 9$. These ranges of reduced velocity are referred to be the initial branches in this study. It can be seen in Fig. 14 that in these ranges of reduced velocity, the response amplitude increases with the reduced velocity. The reduced velocity ranges where the response frequency increases gradually with the reduced velocity to values close to the natural frequency are referred to be lower branches. In the increasing V_r condition, the lower branch is $4 \leq V_r \leq 9.2$, $5.6 \leq V_r \leq 6.6$ and $6 \leq V_r \leq 6.8$ for $\alpha = 0$, 0.5, and 1, respectively. The upper boundary of the lower branch is very clear for $\alpha = 0$ and
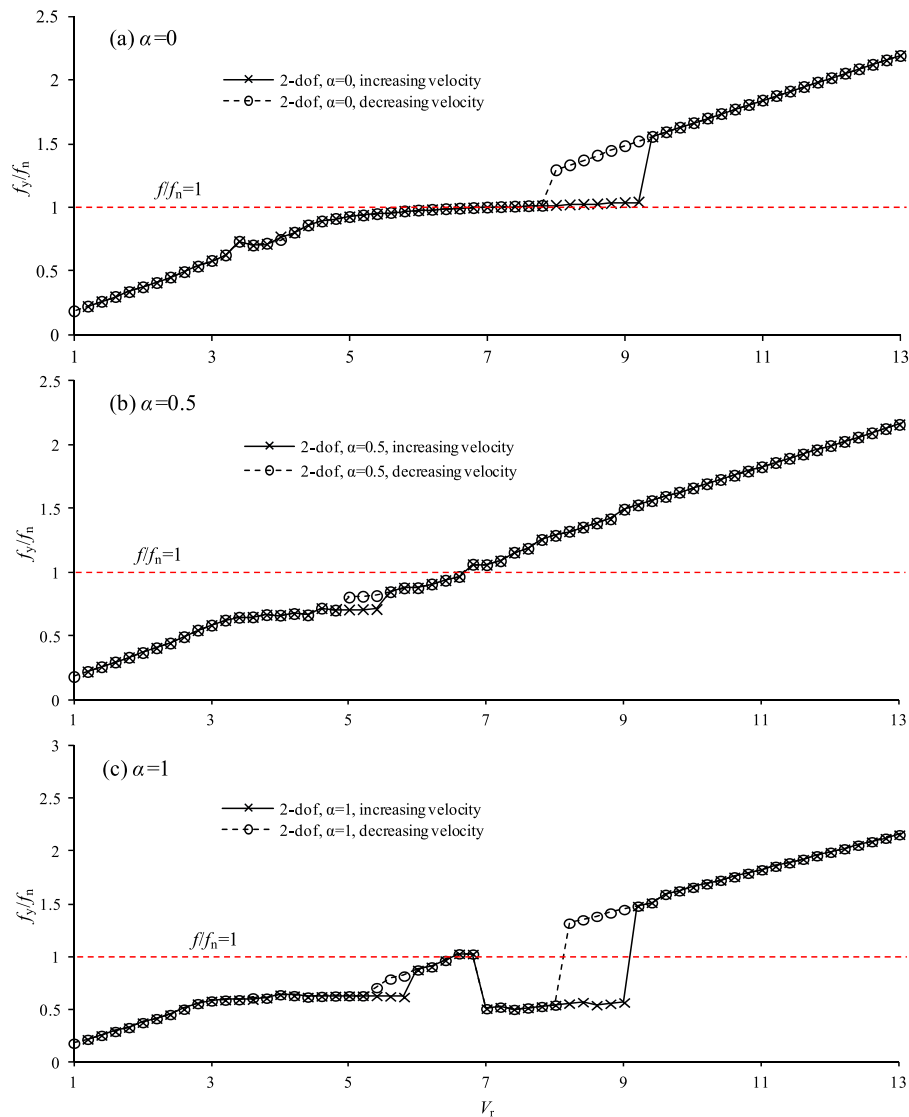
FIG. 15. Variation of the response frequency in the cross-flow direction with the reduced velocity for 2-dof VIV.

1, because both the vibration amplitude and the frequency of the cylinder jumps. For $\alpha = 0.5$, the upper boundary of the lower branch cannot be clearly identified in Fig. 14(b). The reduced velocity of 6.6 is treated to be the upper boundary of the lower branch in the increasing V_r condition because the change rates of the amplitude and the response frequency with reduced velocity change suddenly at this reduced velocity.

Figure 16 shows the variation of the mean position of the cylinder with the reduced velocity under the increasing V_r condition for the 2-dof VIV. Similar to that for the 1-dof VIV, the mean position of the cylinder in the cross-flow direction is negative. The magnitudes of the mean position of the cylinder in both the inline and the cross-flow directions generally increase with V_r. As the reduced velocity exceeds the higher boundary of the initial branch for $\alpha = 0$ (V_r is increased from 5.8 to 6 and from 9 to 9.2), the mean positions of the cylinder in both the inline and the cross-flow directions decrease suddenly. The sudden change in the mean displacement in the cross-flow direction can also be seen at the two ends of the lower branch for $\alpha = 0.5$ ($V_r = 5.6$ and 6.6). It appears that the effect of the rotation rate α on the mean position of the cylinder in the inline direction is weaker than that in the cross-flow direction for $\alpha = 0.5$. Overall, the change rates of
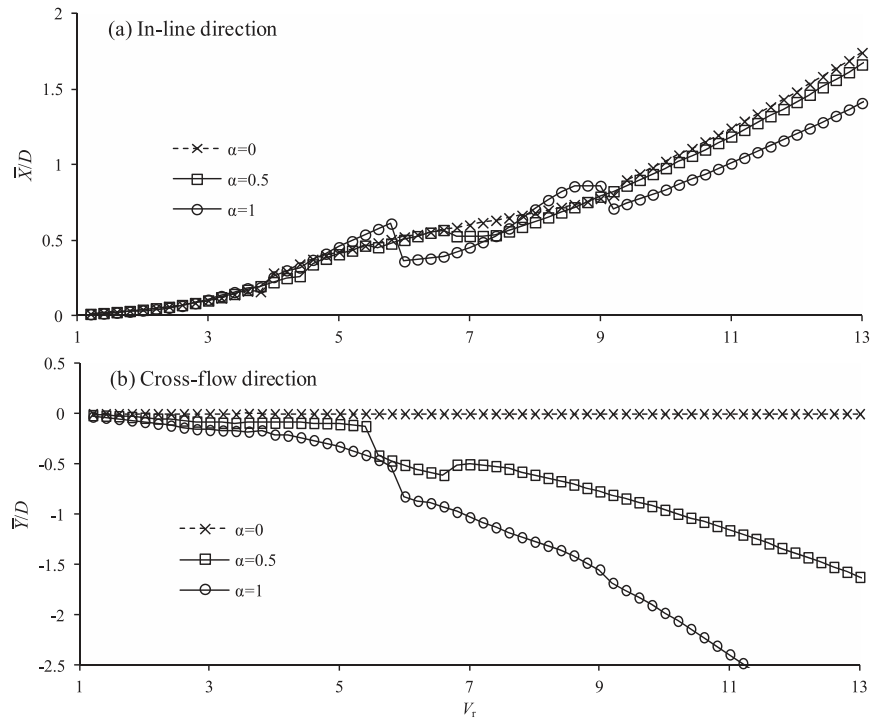
FIG. 16.   Mean position of the cylinder for the 2-dof VIV in the increasing V_r condition.
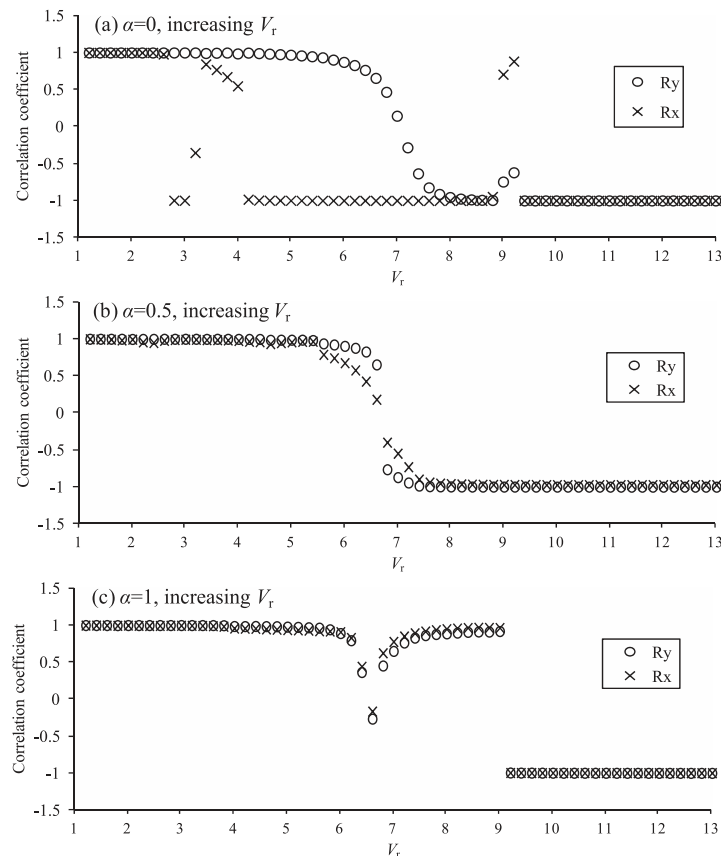

FIG. 17.   Correlation between the force and the displacement for the 2-dof VIV in the increasing V_r condition.
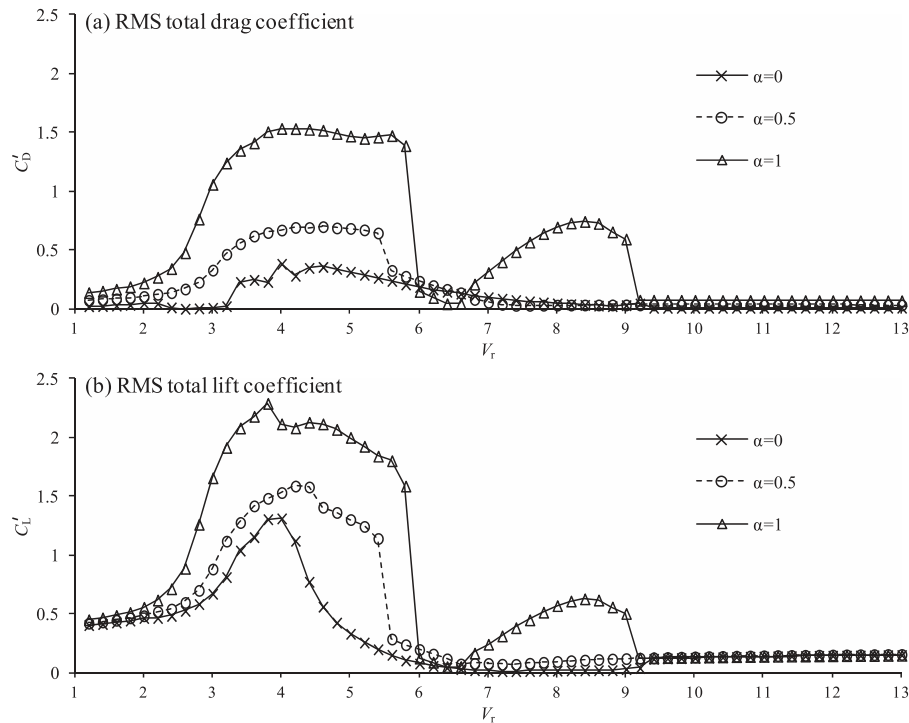
FIG. 18. Variations of the RMS drag and lift coefficients with the reduced velocity for the 2-dof VIV in the increasing V_r condition.

B. Force coefficients and effective added mass coefficients

The correlation coefficients between the vibration displacement and the force coefficient in both the x- and the y-directions are shown in Fig. 17. The variation of the correlation coefficient R_y with V_r for $\alpha = 0$ and 0.5 is similar to their counterparts in the 1-dof VIV. The correlation R_x for $\alpha = 0$ varies between 1 and -1 a number of times as shown in Fig. 17(a). By comparing Fig. 17(a) and Fig. 14(a) it can be seen that whenever the R_x changes from -1 to values close to 1, i.e., the drag force change from out of phase to in phase with the inline displacement, the amplitude in the x-direction increases. The variations of R_x and R_y with the reduced velocity are similar to each other for $\alpha = 0.5$. It can be seen in Fig. 14(b) that the variations of the displacements in the x- and y-directions with the reduced velocity are also similar to each other. The variation of R_y with the reduced velocity for $\alpha = 1$ is very different from those for $\alpha = 0$ and 0.5. The sudden reduction of R_y in the reduced velocity range of $6 \leq V_r \leq 7$ leads to significant reduction in the response amplitude.

Figures 18(a) and 18(b) show the variation of the root mean square (RMS) drag and lift coefficients (C'_D and C'_L) with the reduced velocity for the 2-dof VIV under the increasing V_r condition, respectively. The increase in the rotation rate α leads to significant increase in both the drag and lift coefficients. The increased drag and lift coefficients on a rotating cylinder correspond to the increase in the response amplitudes. Another reason why the maximum response amplitude increases with the increasing rotation rate is because the initial branch, where the response amplitude increases with the increasing V_r, is widened significantly.

Of the total force, only the component that is in phase with the velocity of the cylinder excites the vibration. Figure 19 shows the variation of the time averaged force coefficients that are in phase with the velocities of the cylinder for 2-dof VIV in the increasing V_r condition. The pressure and
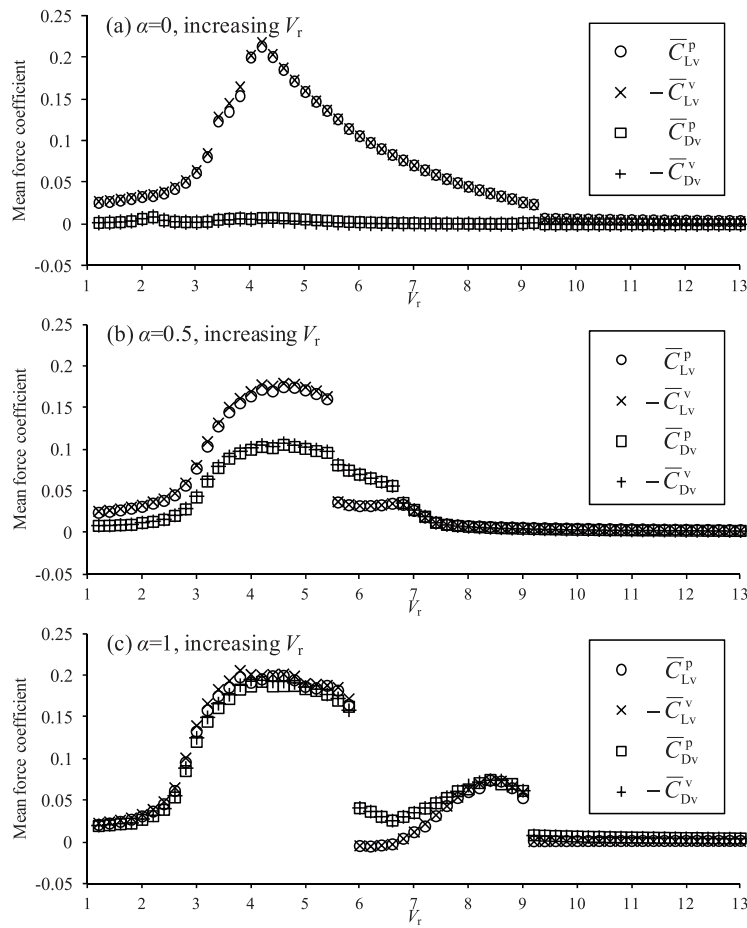
FIG. 19. Variation of the time averaged force coefficients that are in phase with the velocities of the cylinder for 2-dof VIV in the increasing V_r condition.
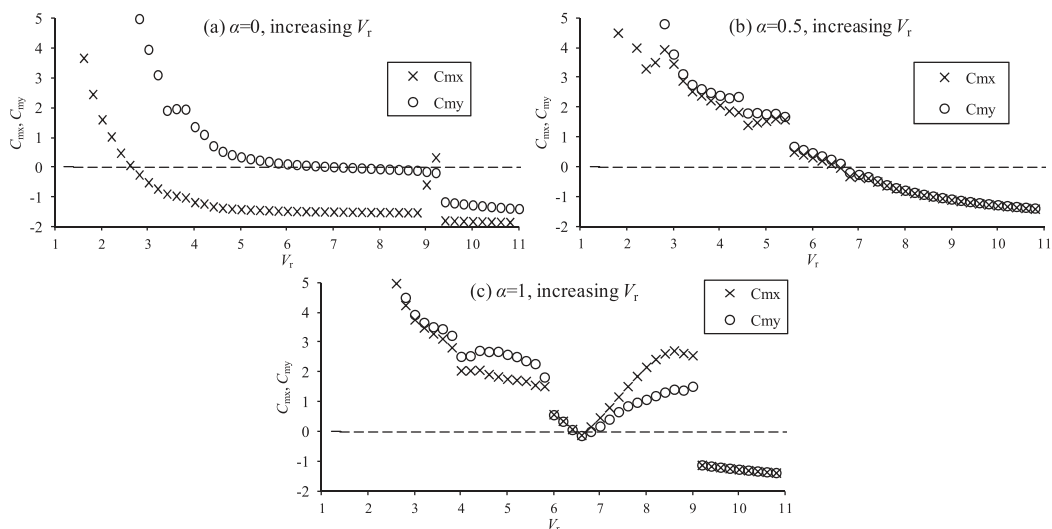

FIG. 20. Variations of the effective added mass with the reduced velocity for the 2-dof VIV in the increasing Vr condition.
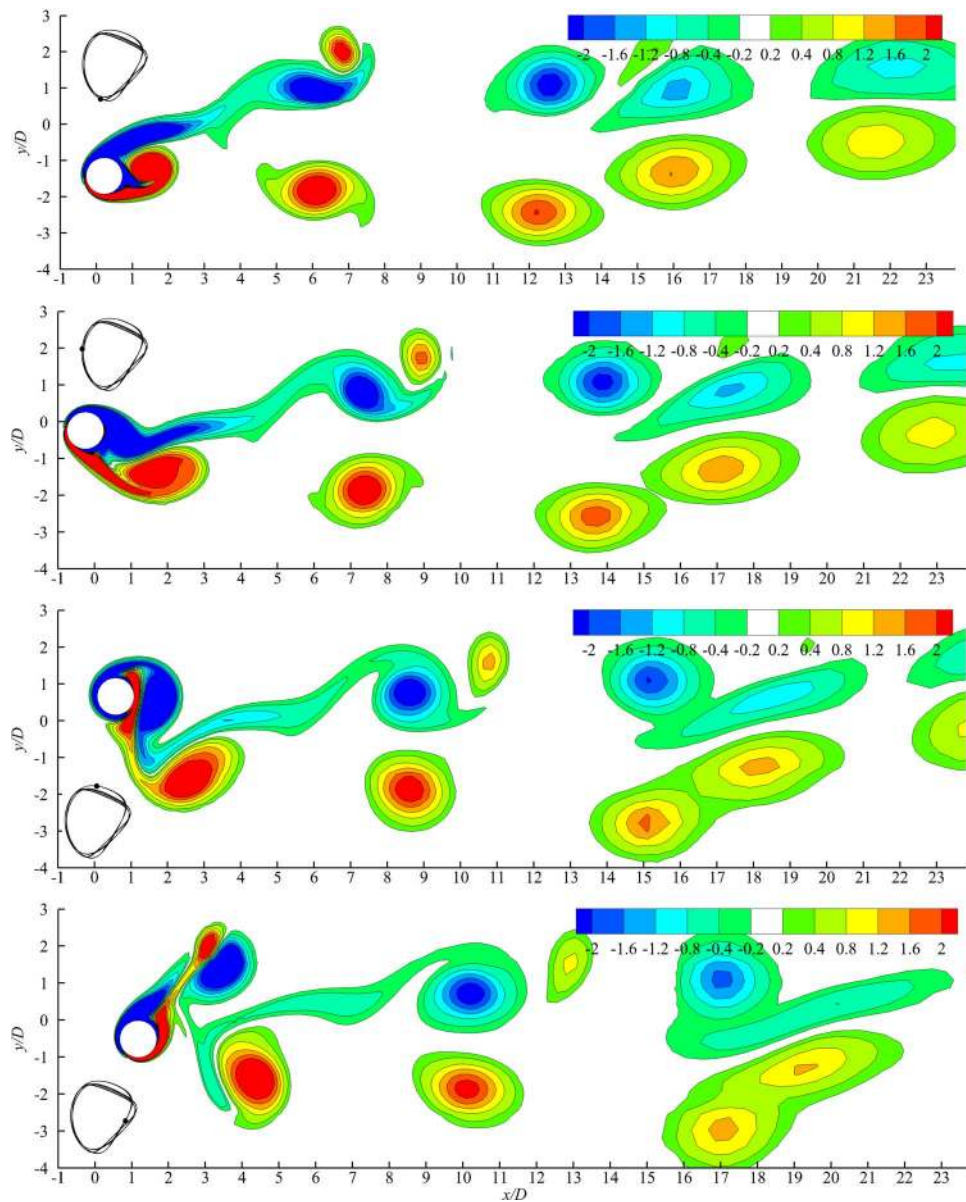
FIG. 21. Contours of the vorticity for the 2-dof VIV at $\alpha = 1$ and $V_r = 5.4$ under the increasing V_r condition.

the viscous components of the drag coefficient that are in phase with the velocity of the cylinder are defined as C_{Dv}^p and C_{Dv}^v, respectively. As in the 1-dof VIV, the pressure force excites the vibration and the force damps the vibration in both the inline and the cross-flow directions. Negative values of $\bar{C}_{Lv}^v$ and $\bar{C}_{Dv}^v$ are plotted in Fig. 19 for the convenience of comparison. Disconnections in the excitation force coefficients are observed at the upper boundaries of the initial branches for $\alpha = 0.5$ and 1 ($V_r = 5.4$ for $\alpha = 0.5$ and $V_r = 5.8$ and 9 for $\alpha = 1$). For $\alpha = 0$, the small jump of the mean force coefficients at the upper boundary of the initial branch (V_r increases from 3.8 to 4) can also be seen in Fig. 19(a). Although the mean total force coefficient that are in phase with the velocity of the cylinder is zero, the magnitudes of the excitation pressure and viscous force coefficients in the lock-in regimes are significantly greater than their counterparts outside the lock-in regimes. This is the reason for the increase of the vibration amplitude in the lock-in regime.

The variations of the effective added mass coefficients in the x- and y-directions are presented in Fig. 20. As in the 1-dof VIV, the added mass coefficients generally decrease with the increasing
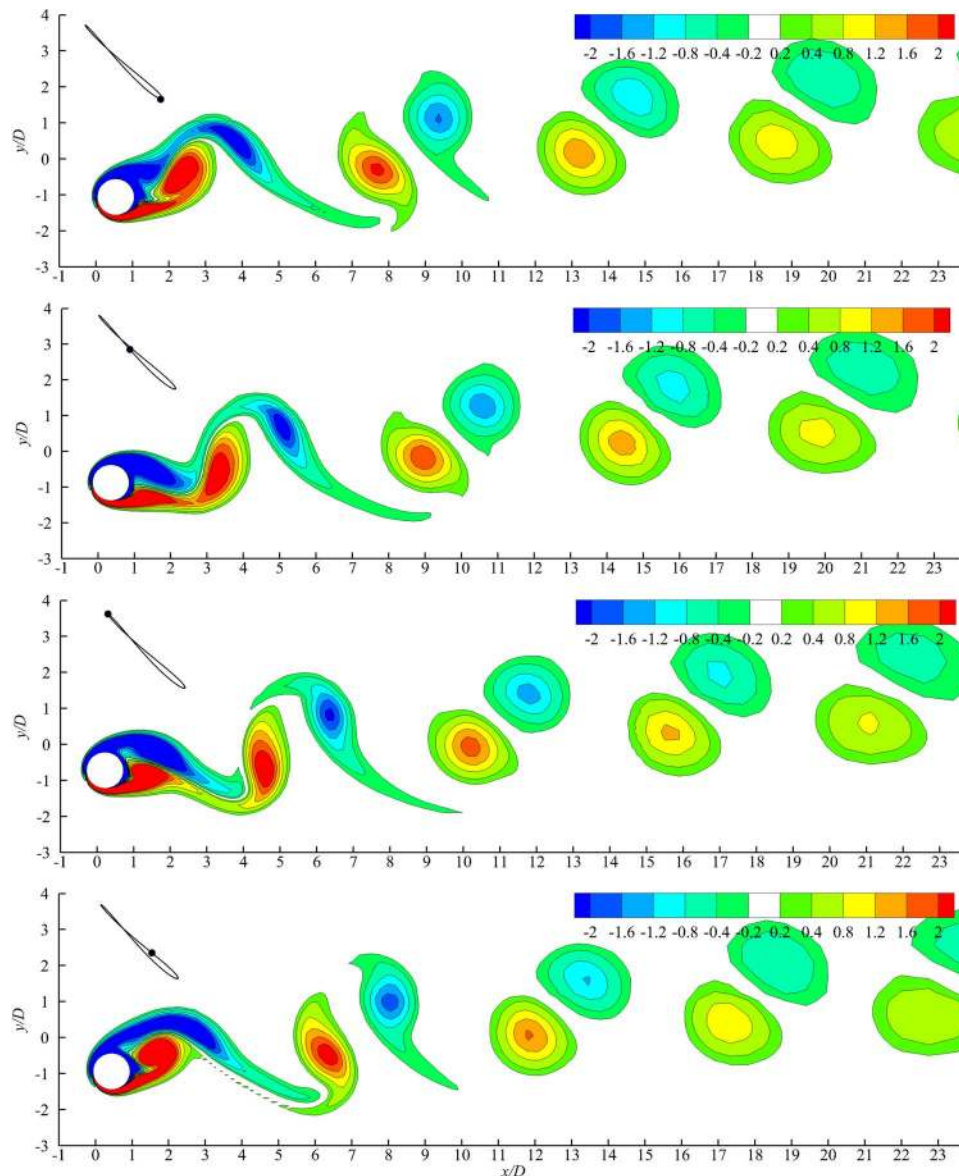
FIG. 22. Contours of the vorticity for the 2-dof VIV under the increasing velocity condition at $\alpha = 1$ and $V_r = 6.4$.

reduced velocity except in the second initial branch for $\alpha = 1$. Disconnection occurs at the boundaries of the response branches. If a response is sinusoidal, the effective added mass coefficients is related to the response frequency as $f/f_n = \sqrt{m^*/(m^* + C_m)}$, where f and C_m stands for the vibration frequency and the added mass coefficient in either the x- or the y-direction. Based on the XY-trajectories in the shape of "8", the vibration frequency in the x-direction is twice that in the y-direction for $\alpha = 0$. Because of this, the effective mass coefficient in the x-direction is smaller than that in the y-direction for $\alpha = 0$. The one-loop XY-trajectories for $\alpha = 0.5$ and 1 indicate that the fundamental vibration frequencies in the x- and the y-directions are the same. However, the slight difference between the added mass coefficients in the x- and the y-directions occurs for $\alpha = 0.5$ because the vibration is not exactly sinusoidal, and this difference becomes strong for $\alpha = 1$. The correlation between the added mass coefficient and the response can be seen by observing Figs. 14, 15, and 20. For instance, the lock-in of the response frequency to an almost constant value in the range of $3.4 \leq V_r \leq 3.8$ corresponds to the constant added mass coefficient in the same range of reduced velocity. Instead of being constant as the response frequency, the added mass coefficients
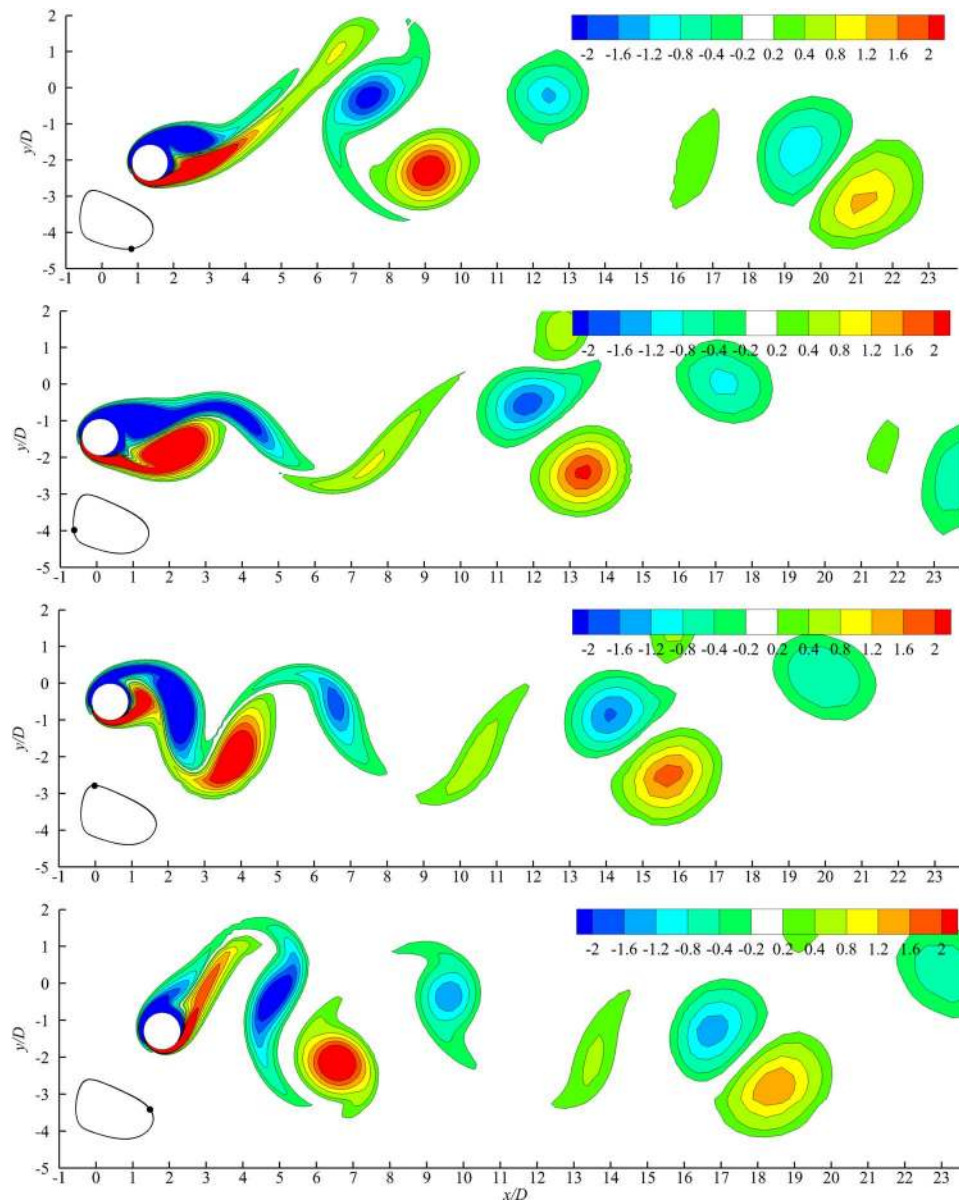
FIG. 23. Contours of the vorticity for the 2-dof VIV under the increasing velocity condition at $\alpha = 1$ and $V_r = 8.6$.

in both the x- and the y-directions decrease slowly with the reduced velocity in the initial branch $3.2 \leq V_r \leq 5.4$ for $\alpha = 0.5$ and the first initial branch ($3 \leq V_r \leq 5.8$) for $\alpha = 1$, probably because the response is not sinusoidal. Bourguet and Jacono[23] reported that when a response is not sinusoidal, the effective added mass coefficient has difference from the one predicted by assuming the response to be sinusoidal. For $\alpha = 1$, the added mass coefficient in the second initial branch increases with the increasing reduced velocity, although the response frequency changes little. This is because the response is very different from a sinusoidal response as shown in Fig. 19(d). Whenever the effective added mass coefficient is zero, the response frequency becomes the same as the natural frequency.

C. Vortex shedding flow patterns

Figure 21 shows the vorticity contours of the wake for $\alpha = 1$ and $V_r = 5.4$, where the response amplitude is the maximum in the first initial branch under the increasing V_r condition. The
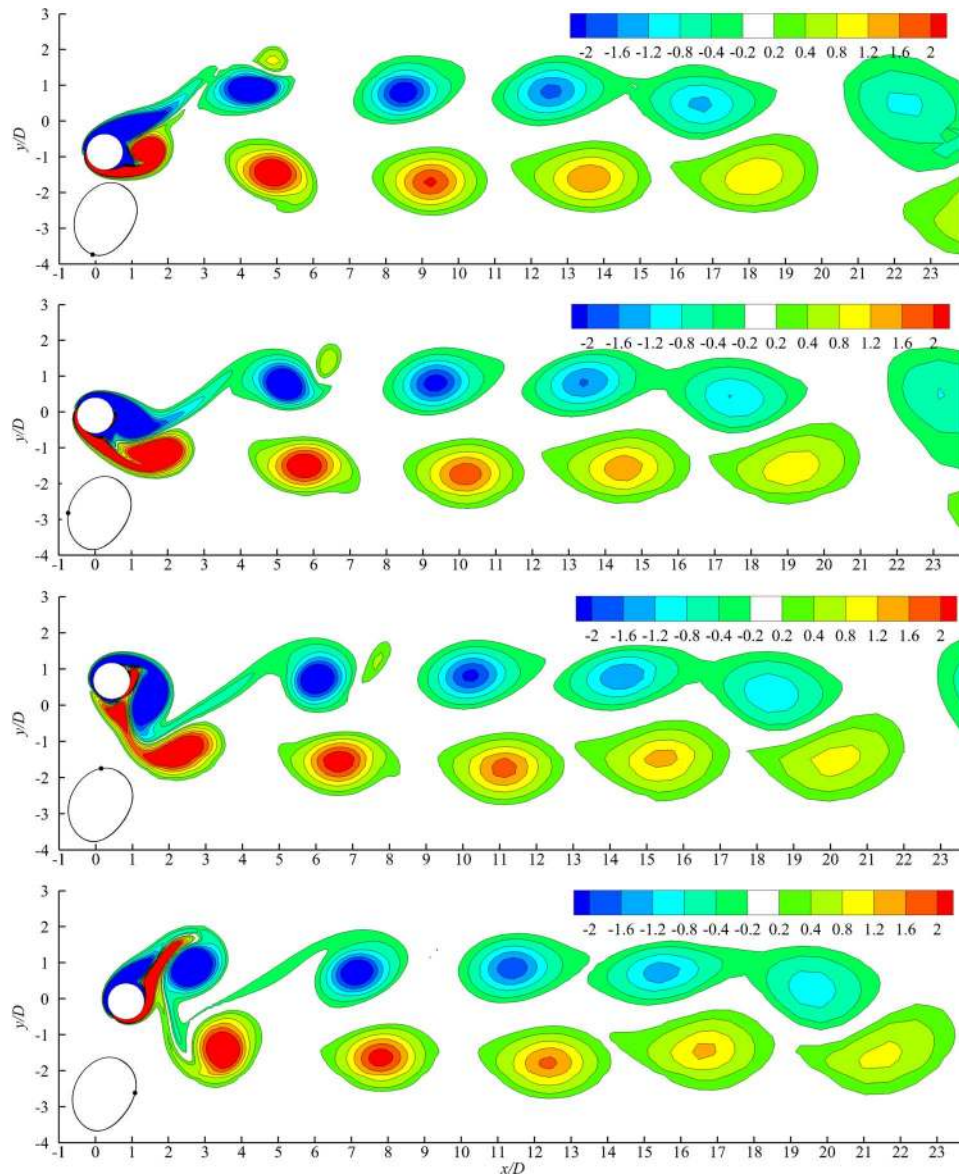
FIG. 24. Contours of the vorticity for the 2-dof VIV under the increasing velocity condition for $\alpha = 0.5$ and $V_r = 5.4$.

instantaneous position of the cylinder on the *XY*-trajectory is shown in each diagram in Fig. 21. The vortex shedding flow, which is asymmetric due to the rotation of the cylinder, is found to be in the P+S mode, i.e., one pair of vortices and one single vortex are shed from the cylinder in one period of vibration. When the cylinder moves from its lowest position to its highest position, one positive vortex is shed from the bottom side of the cylinder as shown in Fig. 21(b). One negative vortex starts to be shed from the cylinder as the cylinder is at its highest position as shown in Fig. 21(c). When the cylinder moves from its highest to its lowest position, a small positive vortex is shed from the cylinder as shown in Fig. 21(d). This small positive vortex dissipates out as *x/D* exceeds 20. Govardhan and Williamson (2000) also found that, in each pair of the vortices in the 2P vortex shedding mode, the second vortex is smaller than the first one.

Figure 22 shows the vorticity contours of the wake flow under the increasing velocity condition at $\alpha = 1$ and $V_r = 6.4$, which is in the lower branch between the two upper branches. The vortex shedding is in the 2S mode, i.e., two vortices are shed from the cylinder in one period of

vibration. Because of the rotation of the cylinder, the vortex street in the wake of the cylinder is aligned above $y/D = 0$ line. The vortices in the wake of the cylinder are in pairs and are regularly arranged.

Figure 23 shows the vorticity contours of wake flow under the increasing velocity condition at $\alpha = 1$ and $V_r = 8.6$, where the response amplitude is the highest in the second upper branch. Similar to the vortex shedding mode observed in Fig. 21, the vortex shedding mode in Fig. 23 is in the P+S mode. However, the formation of the vortices in the wake of the cylinder is found to be different from that in Fig. 21. The shear layers in Fig. 23 from the top and bottom sides of the cylinder extend further downstream before they form vortices, in contrast to those in Fig. 21. The delay in the formation of the vortices contributes to the smaller drag and lift coefficients in the second upper branch than those in the first upper branch. The timing of the vortex shedding in Fig. 23 is not the same as that in Fig. 21. For example, the small positive vortex is shed from the cylinder when the cylinder is at its lowest position in Fig. 23, while it is shed when the cylinder is moving down in Fig. 21.

Figure 24 shows the vorticity contours of the wake flow under the increasing velocity condition for $\alpha = 0.5$ and $V_r = 5.4$, where the response amplitude is the maximum in the upper branch. The pattern of the vortex shedding flow in Fig. 24 is very similar to that at $\alpha = 1$ shown in Fig. 17. However, the small positive vortex that is shed from the cylinder in Fig. 24 is weaker than that in Fig. 17. At $\alpha = 0$, the vortex shedding in the whole lock-in regime becomes 2S mode and the vortex shedding is very similar to that shown in Fig. 22 and is not shown here.

VI. CONCLUSIONS

Vortex-induced vibration of a rotating circular cylinder at a low Reynolds number of 150 and a low mass ratio of 2 is studied numerically. Simulations are conducted for three rotation rates of 0, 0.5, and 1 and reduced velocities in the range of 1 to 13 with an interval of 0.2.

For 1-dof VIV, the rotation of the cylinder widens the lock-in regime and also increases the response amplitude in the lock-in regime. Apart from the widened lock-in regime and the increased response amplitude, the variations of the response amplitude and the frequency with the reduced velocity for $\alpha = 0$, 0.5, and 1 are similar to each other. The mean position of the cylinder in the 1-dof VIV is negative and its magnitude increases with α.

For $\alpha = 0$, the response of the cylinder in the 2-dof VIV is very similar to that in the 1-dof VIV and the response amplitude in the inline direction is significantly smaller than that in the cross-flow direction. When the rotation rate is increased to 0.5 and 1, the response of the cylinder in the 2-dof VIV is changed significantly. For $\alpha = 0.5$ and 1, both the drag coefficient and the response amplitude in the inline direction are increased significantly and become comparable with their counterparts in the cross-flow direction. The response amplitudes in the cross-flow direction for $\alpha = 0.5$ and 1 are also increased significantly compared with that for $\alpha = 0$. No obvious upper branches in the variation of the response amplitude with the reduced velocity are observed for $\alpha = 0$, 0.5, and 1. For $\alpha = 1$, two initial branches are observed and the maximum amplitude in the cross-flow direction in the first initial branch is about 60% higher than that for $\alpha = 0$. The shape "8" vibration *XY*-trajectory in the lock-in regime at $\alpha = 0$ is changed to the single looped *XY*-trajectory at $\alpha = 0.5$ and 1, suggesting that the vibration frequency in the inline direction is the same as that in the cross-flow direction.

By analysing the force component that are in phase with the velocity of the cylinder, it is found that the pressure force excites the vibration and the viscous force damping the vibration in both 1-dof and 2-dof VIVs. Because the damping ratio is zero in this study, the time-averaged total force that is in phase with the velocity of the cylinder is zero, resulting a zero energy transfer from the fluid to the cylinder.

The vortex shedding in the initial branches for $\alpha = 0.5$ and 1 are found to be in the P+S mode, with two positive vortices and one negative vortex are shed from the cylinder in one period of vibration. In the lower branch and outside the lock-in regime, the vortex shedding is in the 2S mode. The vortex shedding in the 1-dof VIV for $\alpha = 0$, 0.5, and 1 and that in the 2-dof VIV for $\alpha = 0$ is always in the 2S mode, regardless inside or outside the lock-in regime.

ACKNOWLEDGMENTS

[1] C. H. K. Williamson, "Vortex dynamics in the cylinder wake," Annu. Rev. Fluid Mech. **28**, 477–539 (1996).

[2] D. Barkley and R. D. Henderson, "Three-dimensional Floquet stability analysis of the wake of a circular cylinder," J. Fluid Mech. **322**, 215–241 (1996).

[3] G. D. Miller and C. H. K. Williamson, "Control of three-dimensional phase dynamics in a cylinder wake," Exp. Fluids **18**, 26–35 (1994).

[4] D. J. Tritton, "Experiments on the flow past a circular cylinder at low Reynolds numbers," J. Fluid Mech. **6**, 547–567 (1959).

[5] C. H. K. Williamson, "The existence of two stages in the transition to three-dimensionality of a cylinder wake," Phys. Fluids **31**, 3165–3168 (1988).

[6] H. Zhang, U. Fey, B. R. Noack, M. König, and H. Eckelmann, "On the transition of the cylinder wake," Phys. Fluids **7**(4), 779–794 (1995).

[7] C. H. K. Williamson, "Three-dimensional wake transition," J. Fluid Mech. **328**, 345–407 (1995).

[8] A. Prasad and C. H. K. Williamson, "Three-dimensional effect in turbulent bluff-body wakes," J. Fluid Mech. **343**, 235–265 (1997).

[9] M. Zhao, J. Thapa, L. Cheng, and T. Zhou, "Three-dimensional transition of vortex shedding flow around a circular cylinder at right and oblique attacks," Phys. Fluids **25**, 014105 (2013b).

[10] F. Diaz, J. Gavalda, J. G. Kawall, J. F. Keller, and F. Giralt, "Vortex shedding from a spinning cylinder," Phys. Fluids **26**, 3454–3460 (1983).

[11] H. M. Badr, M. Coutanceau, S. C. R. Dennis, and C. Menard, "Unsteady flow past a rotating circular cylinder at Reynolds numbers 10^3 and 10^4," J. Fluids Mech. **220**, 459–484 (1990).

[12] C. C. Chang and R. L. Chern, "Vortex shedding from an impulsively started rotating and translating circular cylinder," J. Fluid Mech. **233**, 265–298 (1991).

[13] Y. T. Chew, M. Cheng, and S. C. Luo, "A numerical study of flow past a rotating circular cylinder using a hybrid vortex scheme," J. Fluid Mech. **299**, 35–71 (1995).

[14] M. H. Chou, "Numerical study of vortex shedding from a rotating cylinder immersed in a uniform flow field," Int. J. Numer. Methods Fluids **32**, 545–567 (2000).

[15] H. M. Badr, S. C. R. Dennis, and P. J. S. Young, "Steady and unsteady flow past a rotating circular cylinder at low Reynolds numbers," Comput. Fluids **17**(4), 579–609 (1989).

[16] T. Tang and D. B. Ingham, "On steady flow past a rotating circular cylinder at Reynolds numbers 60 and 100," Comput. Fluids **19**(2), 217–230 (1991).

[17] S. Kang, H. Choi, and S. Lee, "Laminar flow past a rotating circular cylinder," Phys. Fluids **11**, 3312–3321 (1999).

[18] S. J. Karabelas, "Large eddy simulation of high-Reynolds number flow past a rotating cylinder," Int. J. Heat Fluid Flow **31**, 518–527 (2010).

[19] D. Stojkovic, M. Breuer, and F. Durst, "Effect of high rotation rates on the laminar flow around a circular cylinder," Phys. Fluids **14**, 3160–3178 (2002).

[20] J. Pralits, L. Brandt, and F. Giannetti, "Instability and sensitivity of the flow around a rotating circular cylinder," J. Fluid Mech. **650**, 513–536 (2010).

[21] S. Mittal and B. Kumar, "Flow past a rotating cylinder," J. Fluid Mech. **476**, 303–334 (2003).

[22] L. Lu, J. M. Qin, B. Teng, and Y. C. Li, "Numerical investigations of lift suppression by feedback rotary oscillation of circular cylinder at low Reynolds number," Phys. Fluids **23**, 033601 (2011).

[23] R. Bourguet and D. L. Jacono, "Flow-induced vibrations of a rotating cylinder," J. Fluid Mech. **740**, 342–380 (2014).

[24] T. Sarpkaya, "Vortex-induced oscillations: A selective review," J. Appl. Mech. **46**, 241–258 (1979).

[25] J. M. Dahl, F. S. Hover, M. S. Triantafyllou, and O. H. Oakley, "Dual resonance in vortex-induced vibrations at subcritical and supercritical Reynolds numbers," J. Fluid Mech. **643**, 395–424 (2010).

[26] K. Vikestad, J. K. V. Andiver, and C. M. Larsen, "Added mass and oscillation frequency for a circular cylinder subjected to vortex-induced vibrations and external disturbance," J. Fluids Struct. **14**, 1071–1088 (2000).

[27] K. M. Lam, "Vortex shedding flow behind a slowly rotating circular cylinder," J. Fluids Struct. **25**, 245–262 (2009).

[28] S. Mittal, "Three-dimensional instabilities in flow past a rotating cylinder," J. Appl. Mech. **71**, 89–95 (2004).

[29] R. E. L. Akoury, M. Braza, R. Perrin, G. Harran, and Y. Hoarau, "The three-dimensional transition in the flow around a rotating cylinder," J. Fluid Mech. **607**, 1–11 (2008).

[30] A. Rao, J. Leontini, M. C. Thompson, and K. Hourigan, "Three-dimensionality in the wake of a rotating cylinder in a uniform flow," J. Fluid Mech. **717**, 1–29 (2013).

[31] P. W. Bearman, "Vortex shedding from oscillating bluff_bodies," Annu. Rev. Fluid Mech. **16**, 195–222 (1984).

[32] A. Okajima, "Brief review: Numerical analysis of the flow around vibrating cylinders," J. Wind Eng. Indus. Aerodyn. **46 and 47**, 881–884 (1993).

[33] B. M. Sumer and J. Fredsøe, *Hydrodynamics Around Cylindrical Structures* (World Scientific, 1997).

[34] T. Sarpkaya, "A critical review of the intrinsic nature of vortex-induced vibrations," J. Fluids Struct. **19**(4), 389–447 (2004).

[35] C. H. K. Williamson and R. Govardhan, "Vortex-induced vibrations," Annu. Rev. Fluid Mech. **36**, 413–455 (2004).

[36] C. H. K. Williamson and R. Govardhan, "A brief review of recent results in vortex-induced vibrations," J. Wind Eng. Indus. Aerodyn. **96**, 713–735 (2008).

[37] C. H. K. Williamson and A. Roshko, "Vortex formation in the wake of an oscillating cylinder," J. Fluids Struct. **2**, 355–381 (1988).

[38] A. Khalak and C. H. K. Williamson, "Dynamics of a hydroelastic cylinder with very low mass and damping," J. Fluids Struct. **10**, 455–472 (1996).

[39] A. Khalak and C. H. K. Williamson, "Motions, force and mode transitions in vortex-induced vibrations at low mass-damping," J. Fluids Struct. **13**, 813–851 (1999).

[40] N. Jauvtis and C. H. K. Williamson, "The effect of two degrees of freedom on vortex-induced vibration at low mass and damping," J. Fluid Mech. **509**, 23–62 (2004).

[41] R. Govardhan and C. H. K. Williamson, "Modes of vortex formation and frequency response of a freely vibrating cylinder," J. Fluid Mech. **420**, 85–130 (2000).

[42] S. P. Singh and S. Mittal, "Vortex-induced oscillations at low Reynolds numbers: Hysteresis and vortex-shedding modes," J. Fluids Struct. **20**, 1085–1104 (2005).

[43] M. Zhao, L. Cheng, and T. Zhou, "Numerical simulation of vortex-induced vibration of a square cylinder at a low Reynolds number," Phys. Fluids **25**, 023603 (2013).

[44] C. C. Feng, "The measurements of vortex-induced effects on flow past a stationary and oscillation and galloping," M.S. thesis (University BC, Vancouver, Canada, 1968).

[45] M. Zhao, "Flow induced vibration of two rigidly coupled circular cylinders in tandem and side-by-side arrangements at a low Reynolds number of 150," Phys. Fluids **25**, 123601 (2013).

[46] M. Zhao and G. Yan, "Numerical simulation of vortex-induced vibration of two circular cylinders of different diameters at low Reynolds number," Phys. Fluids **25**, 083601 (2013).

[47] M. Zhao, F. Tong, and L. Cheng, "Numerical simulation of two-degree-of-freedom vortex-induced vibration of a circular cylinder between two lateral plane walls in steady currents," J. Fluids Eng. **134**, 104501 (2012).

[48] T. K. Prasanth, S. Behara, S. P. Singh, R. Kumar, and S. Mittal, "Effect of blockage on vortex-induced vibrations at low Reynolds numbers," J. Fluids Struct. **22**, 865–876 (2006).

[49] M. Coutanceau and C. Menard, "Influence of rotation on the near wake development behind an impulsively started circular cylinder," J. Fluid Mech. **158**, 399–466 (1985).

[50] J. C. Padrino and D. D. Joseph, "Numerical study of the steady-state uniform flow past a rotating cylinder," J. Fluid Mech. **557**, 191–223 (2006).

[51] D. Stojkovic, P. Schon, M. Breuer, and F. Durst, "On the new vortex shedding mode past a rotating circular cylinder," Phys. Fluids **15**, 1257–1260 (2003).

[52] Y. Bao, D. Zhou, and J. Tu, "Flow interference between a stationary cylinder and an elastically mounted cylinder arranged in proximity," J. Fluids Struct. **27**, 1425–1446 (2011).

[53] I. Borazjani and F. Sotiropoulos, "Vortex-induced vibrations of two cylinders in tandem arrangement in the proximity-wake interference region," J. Fluid Mech. **621**, 321–364 (2009).

[54] J. S. Leontini, M. C. Thompson, and K. Hourigan, "The beginning of branching behaviour of vortex-inducedvibration during two-dimensional flow," J. Fluids Struct. **22**, 857–864 (2006).

[55] S. Mittal and V. Kumar, "Finite element study of vortex-induced cross-flow and in-line oscillations of a circular cylinder at low Reynolds numbers," Int. J. Numer. Methods Fluids **31**, 1087–1120 (1999).

[56] I. Ghazanfarian and M. R. H. Nobari, "A numerical study of convective heat transfer from a rotating cylinder with cross-flow oscillation," Int. J. Heat Mass Transfer **52**, 5402–5411 (2009).

[57] T. L. Morese and C. H. K. Williamson, "Prediction of vortex-induced vibration response by employing controlled motion," J. Fluid Mech. **634**, 5–39 (2009).

[58] A. Sanchis, G. Sælevik, and J. Grue, "Two-degree-of-freedom vortex-induced vibrations of a spring-mounted rigid cylinder with low mass ratio," J. Fluids Struct. **24**, 907–919 (2008).

[59] C. Ji, Z. Xiao, Y. Wang, and H. Wang, "Numerical investigation on vortex-induced vibration of an elastically mounted circular cylinder at low Reynolds number using the fictitious domain method," Int. J. Comput. Fluid Dyn. **25**(4), 207–221 (2011).

[60] P. Anagnostopoulos and P. W. Bearman, "Response characteristics of a vortex-excited cylinder at low Reynolds numbers," J. Fluids Struct. **6**, 39–50 (1992).